PNNL-38275
M3LW-25OR0404015

Light Water Reactor Sustainability Program

Consideration of Decabromodiphenyl Ether Flame Retardant in Thermal and Radiation Aging of Crosslinked Polyethylene Cable Insulation

September 2025

U.S. Department of Energy
Office of Nuclear Energy

DISCLAIMER

This information was prepared as an account of work sponsored by an agency of the U.S. Government. Neither the U.S. Government nor any agency thereof, nor any of their employees, makes any warranty, expressed or implied, or assumes any legal liability or responsibility for the accuracy, completeness, or usefulness, of any information, apparatus, product, or process disclosed, or represents that its use would not infringe privately owned rights. References herein to any specific commercial product, process, or service by trade name, trade mark, manufacturer, or otherwise, does not necessarily constitute or imply its endorsement, recommendation, or favoring by the U.S. Government or any agency thereof. The views and opinions of authors expressed herein do not necessarily state or reflect those of the U.S. Government or any agency thereof.

PNNL-38275
M3LW-25OR0404015

Consideration of Decabromodiphenyl Ether Flame Retardant in Thermal and Radiation Aging of Crosslinked Polyethylene Cable Insulation

Yelin Ni, Md Kamrul Hasan, Tyler R. Tueller, Kumari Sushmita, Maddison A. Rex, Mark K. Murphy, Leonard S. Fifield

September 2025

Prepared by
Pacific Northwest National Laboratory
Richland, WA 99354
for the
U.S. Department of Energy
under Contract DE-AC05-76RL01830

SUMMARY

Decabromodiphenyl ether (decaBDE) has been used as a flame-retardant additive in nuclear-grade electrical cable insulation. However, decaBDE has been identified as a persistent, bioaccumulative and toxic substance, leading to regulatory scrutiny. Since decaBDE has long been relied upon as the flame retardant in one of the most common cross-linked polyethylene (XLPE) nuclear cable insulation formulations, RSCC Firewall® III, questions have naturally arisen regarding whether changes in cable performance might be expected for XLPE containing a decaBDE alternative, especially for safety-related cables that must perform their safety function in a design basis event such as a loss of coolant accident. The research described here directly investigates observable differences in material performance of the standard historical decaBDE-containing XLPE insulation and the newly formulated XLPE containing a decaBDE alternative for samples subjected to accelerated thermal aging. Mechanical properties, thermal oxidative resistance, chemical structures, and discoloration of XLPE samples provided by the manufacturer with and without decaBDE were determined after various thermal and radiation aging conditions. Statistical analyses were performed to test the difference between samples of the two formulations in their measured properties. Key findings from this work include:

- Statistically detectable differences between decaBDE-containing (XLPE-dBDE) and alternative formulation (XLPE-Alt) cable insulation samples were found primarily under sequential aging conditions (T→R, R→T) and thermal-only aging, particularly in yellowness, Fourier-transform infrared spectroscopy response, and mass change metrics. For other material properties such as tensile elongation and carbonyl index, no statistically significant difference was found between the two formulations.
- Antioxidants were effectively protecting the material from thermal degradation, but less effectively consumed during radiation-only aging.
- "Inverse temperature effect" (ITE) observed during radiation-only aging for some samples that were highly brittle (elongation at break [EAB] < 50%) but not for others with the same aging time that remained ductile, indicating that ITE susceptibility is highly localized. Necking and non-uniform strain distribution during the tensile testing was observed for those embrittled samples.
- DecaBDE debromination may contribute to increased yellowing in addition to carbonyl formation, potentially explaining why XLPE-dBDE showed higher yellowness index compared to the alternative formulation.
- Simultaneous thermal and radiation aging (T&R) represented the most degradative scenario for the investigated aging metrics among the different orders of applying heat and radiation. Under the T&R scenario, apparent synergistic acceleration of degradation was observed, rather than simple additive effects from individual thermal and radiation aging conditions.

Statistical differences in aging behavior were observed between the two XLPE formulations in terms of color change, chemical bonding, and mass change. Antioxidant behavior differences were observed in the as-received formulations, but differences went away with aging. No statistical differences between the two formulations were observed in mechanical performance loss due to aging. These observations are consistent with the fact that the XLPE-dBDE and the XLPE-Alt materials have different chemical compositions and do not support the expectation of differences in performance of the safety-related functions of cable constructed from the two formulations.

CONTENTS

LIST OF FIGURES

LIST OF TABLES

ACKNOWLEDGEMENTS

This work was sponsored by the U.S. Department of Energy, Office of Nuclear Energy, for the Light Water Reactor Sustainability (LWRS) program Materials Research Pathway. The authors extend their appreciation to Pathway Lead Dr. Xiang (Frank) Chen and Technical Integration Office Director Dr. Bruce Hallbert for LWRS programmatic support. RSCC Wire & Cable is gratefully acknowledged for provision of directly comparable insulated wires composed of Firewall® III crosslinked polyethylene of the historic formulation containing decabromodiphenyl ether flame retardant and of the crosslinked polyethylene alternative formulation. This work was performed at the Pacific Northwest National Laboratory (PNNL). PNNL is operated by Battelle for the U.S. Department of Energy under contract DE-AC05-76RL01830.

1. INTRODUCTION

1.1 Flame-Retardant Strategies for Nuclear-Grade Cables

Polymers such as crosslinked polyethylene (XLPE) and ethylene propylene rubber (EPR) are widely used as insulations in nuclear-grade cables because they offer excellent dielectric properties and thermal and radiation resistance. Since these materials do not inherently possess optimal flame-retardant (FR) properties, flame retardancy is achieved through two main strategies: (1) adding fire-resistant barriers in a multi-layered cable system, such as FR tapes, sheaths, and jackets; and (2) integrating FR additives into the polymer matrix.

1.1.1 Fire-Resistant Barrier Layers

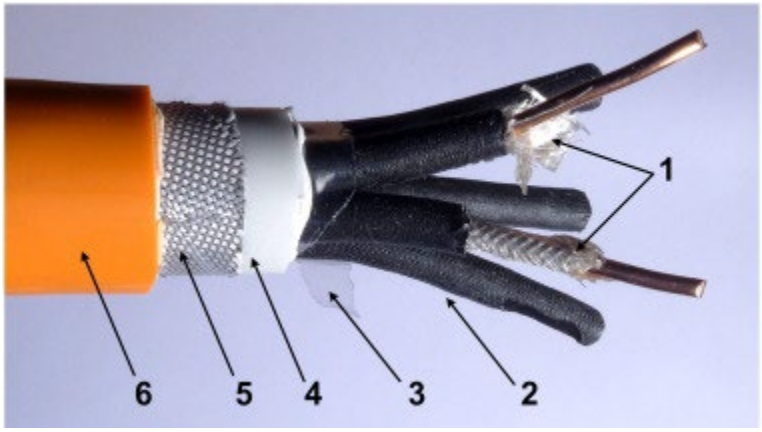

Figure 1. Exposed components of a cable consisting of (1) an FR mica glass tape, (2) an XLPE-type insulation, (3) a polyester film, (4) a low-density polyethylene/ethylene-vinyl acetate (LDPE/EVA) blend filled with aluminum hydroxide (ATH), (5) a woven glass fabric coated with an FR acrylic resin, and (6) an outer sheath of LDPE/EVA blend filled with ATH and orange pigment [1].

The example of multi-layered cable construction shown in Figure 1 consists of three FR layers: a mica glass tape (labeled as “1” in Figure 1), a bedding of low-density polyethylene/ethylene-vinyl acetate (LDPE/EVA) filled with aluminum hydroxide (ATH; labeled as “4” in Figure 1), and a fire-retardant, halogen-free, low-smoke cross-linked acrylic-coated woven glass fabric (labeled as “5” in Figure 1) [1].

The jacketing layer made from intrinsically FR materials contributes to flame retardancy through three mechanisms depending on the base polymer:

1. Halogenated polymers, such as chloroprene rubber, chlorosulfonated polyethylene (CSPE), and chlorinated polyethylene (CPE), achieve flame retardancy primarily by releasing halogen radicals during combustion that interrupt radical chain reactions in the gaseous phase [2, 3].
2. Silicone-based polymers exhibit flame retardancy through a physical mechanism by forming a silica (SiO_2) char layer during combustion that protects the underlying materials from heat and oxygen [2].
3. Fluorocarbons are resistant to ignition due to the high energy (107–116 kcal/mol) of the carbon-fluorine (C-F) bond [4, 5].

1.1.2 Flame-Retardant Additives

The second strategy involves incorporation of FR additives into the polymer matrix, primarily through blending during polymerization or melt compounding processes. While FR additives can also be chemically bonded to the polymer backbone via copolymerization or grafting [6], physical blending is

simpler and more cost-effective, and is favored by industrial applications [7]. Table 1 lists the different categories of FR additives based on chemical structures.

Table 1. General categories of FR additives based on the different chemistries [6–8].

Category	Examples	FR Mechanism	Concerns
Inorganic-based (metal hydroxides, carbonates, hydroxycarbonates, borates)	Aluminum tri-hydroxide (ATH), magnesium di-hydroxide (MDH), magnesium hydroxycarbonate, magnesium carbonate, zinc borates	(1) Release of non-flammable gases (H_2O, CO_2) dilutes the fuel and forms a protective gas layer; (2) heat-sink effect: cool down the polymer through endothermic decomposition of the additive; (3) decomposition products (metal oxides) form a thermally insulating protective coating	High loading is needed due to low FR efficiency, which leads to deterioration of mechanical properties
Halogenated (bromine-based and chlorine-based)	Tetrabromobisphenol A (TBBPA), polybromodiphenylether (PBDE) including penta- (5), octa- (8), and deca- (10) BDEs, hexabromocyclododecane (HBCD), tetrabromophthalic anhydride (TBPA), dechlorane plus (DP)	$RX \rightarrow R^{\bullet} + X^{\bullet}$ X may be Br or Cl $X^{\bullet} + R'H \rightarrow R'^{\bullet} + HX$ $HX + H^{\bullet} \rightarrow H_2 + X^{\bullet}$ $HX + OH^{\bullet} \rightarrow H_2O + X^{\bullet}$ (1) Scavenge highly reactive free-radical species (e.g., H· and OH·) to stop the chain reaction of polymer combustion; (2) HX forms a protective gas layer and dilutes the fuel gases; (3) catalyzes the oxidation of the solid phase to form a protective layer	Certain ones being phased out due to environmental issues and toxicity
Phosphorus-based	Red phosphorus (RP), ammonium polyphosphate (APP), bisphenol A bis(diphenyl phosphate) (BDP), resorcinol bis(diphenyl phosphate) (RDP), aluminum hypophosphite (AP)	(1) PO·, PO_2,· and HPO radicals quench the chain reaction in the gas phase; (2) decomposition of the additives forms acids (e.g., phosphoric acid), which catalyzes dehydration reactions leading to char formation; (3) more effective in polymers that contain oxygen and nitrogen	RP can release toxic phosphine in melt processing
Intumescent system (acid source + carbonizing agent + blowing agent)	Acid source: ammonium salts and phosphates, e.g., ammonium polyphosphate (APP); carbonizing agent: pentaerythritol (PER), polyols; blowing agent: melamine, guanidine, urea, chlorinated paraffins	(1) Acid catalyzes the dehydration of the carbonizing agent to generate char; (2) Blowing agent releases gas to expand the char layer	Conventional APP+PER system: bad processability, migration, poor water resistance
Silicon-based	Silica (SiO_2) gel, block/graft copolymers including silicone segments (e.g., PC-b-PDMS), SiO_2-based and phosphorus-containing organic–inorganic hybrid	(1) Formation of thermally stable ceramic layer (e.g., SiO_2-rich char layer) to inhibit heat release and protect the underlying material; (2) increase limiting oxygen index (LOI)	SiO_2: Low efficiency, poor compatibility with polymer

1.2 Regulatory History of Flame-Retardant Additives

In the United States, the demand for chemical flame retardants rapidly increased in response to the regulatory requirements for fireproof products [9]. In 1977, following research showing that brominated tris [tris(2,3-dibromopropyl) phosphate] is mutagenic, the Consumer Product Safety Commission (CPSC) banned its use in sleepwear for children—an enforcement move that later resulted in several lawsuits despite the ban being reversed on procedural grounds [9, 10].

The Toxic Substances Control Act (TSCA) of 1976 emerged as the principal federal framework. Under TSCA, the Environmental Protection Agency (EPA) has developed policy, including Significant New Use Rules (SNURs), to restrict chemicals like decabromodiphenyl ether (decaBDE) and other polybrominated diphenyl ethers (PBDEs) [10, 11]. Key regulatory actions include:

- In 2003, ten states enacted bans on penta- and octa-BDE formulations in consumer products [12].
- In 2010, EPA announced a voluntary phase-out of decaBDE in electrical, electronic, and plastic applications, targeting completion by 2013 [12].
- In 2021, EPA implemented a rule under TSCA Section 6(h) targeting decaBDE for its persistent, bioaccumulative, and toxic (PBT) characteristics, restricting its use in consumer products [13].

Regulatory actions by local legislation and agencies worldwide regarding flame retardants are summarized in Table 2.

Table 2. Regulatory actions refining the applications of flame retardants.

Year	Agency, Act	Targeted flame retardants
2004	European Union, Regulation (EC) No. 850/2004 [the Persistent Organic Pollutants (POPs) Regulation]	Banned production, marketing, and use of PBDE with narrowly defined exemptions for recycled materials and certain electronic equipment [14]
2007	European Chemicals Agency (ECHA), operating under the EU Registration, Evaluation, Authorization and Restriction of Chemicals (REACH) regulation	Hexabromocyclododecane (HBCD) and Tris(2-chloroethyl) phosphate (TCEP) were placed on the Candidate List as Substances of Very High Concern (SVHC) [11]
2008	Environment Canada, Polybrominated Diphenyl Ethers Regulations	Banned the manufacture of PBDEs and reached a voluntary agreement with key producers to phase out their use across electrical and electronic equipment, transportation, and military applications [14]
2016	Washington, D.C. Law 21-108, the Carcinogenic Flame Retardant Prohibition Amendment Act	Carcinogenic FRs, including PBDEs, organophosphates (TCEP, TCPP, TDCPP) [15]

1.3 EPA Regulation of decaBDE in Nuclear-Grade Cables

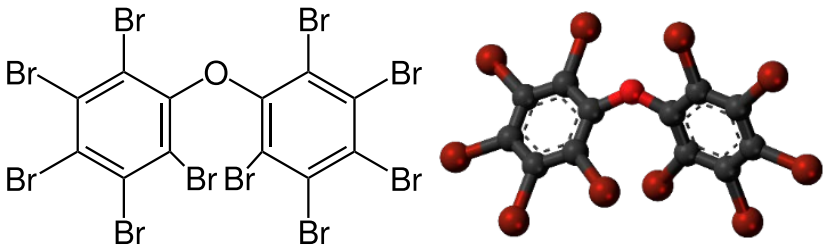

Figure 2. Chemical structure of decabromodiphenyl ether (decaBDE).

EPA initiated regulatory actions to phase out decaBDE-containing materials due to its PBT properties. In 2019, EPA published a proposed rule addressing five PBT chemicals including decaBDE. The proposed rule would "restrict or prohibit manufacture (including import), processing, and distribution in commerce" of decaBDE or decaBDE-containing products or articles, and set a compliance deadline of 60 days after final rule publication with exceptions for aerospace and hospitality industries [16].

Nuclear-grade cables are designed to withstand extreme conditions and meet stringent fire safety and performance standards. Historically, decaBDE was chosen for its ability to meet these standards while maintaining cost efficiency in production. A sudden unavailability of decaBDE-containing cables, especially the Class 1E cables used in safety-related systems, would disrupt the supply of alternative, non-decaBDE cables for continued operation and scheduled maintenance of nuclear power plants [17]. Qualification of alternative formulations could take years, potentially exacerbating supply chain disruptions [18, 19]. After engaging with RSCC Wire & Cable, LLC (RSCC), the primary supplier of decaBDE-containing cables, EPA published the final rule where an extended compliance deadline of January 6, 2023 was included for "processing and distribution in commerce of decaBDE for use in wire and cable insulation in nuclear power generation facilities, and for decaBDE-containing wire and cable insulation" [13, 17, 19].

On May 2, 2023, in recognition of the potential supply chain disruptions and industry concerns following abrupt discontinuation of decaBDE-containing Class 1E wire and cable essential for nuclear power operations after the January 6, 2023 compliance deadline, and the time needed for qualifying the individual components using the alternative insulation technology, EPA issued an "enforcement statement regarding the prohibition of processing and distribution in commerce of decabromodiphenyl ether (decaBDE)-containing wire and cable insulation in nuclear power generation facilities under 40 C.F.R. § 751.405(a)(2)(ii)," granting enforcement discretion for the nuclear industry and their suppliers until September 30, 2024, provided the entities were "working diligently to qualify their alternative components under NRC (Nuclear Regulatory Commission) regulations and guidance" [17, 18, 20, 21]. EPA extended this discretion until January 30, 2025, through an updated statement published on September 27, 2024 [22].

On November 12, 2024, the EPA finalized amendments to the 2021 decaBDE rule to address ongoing compliance challenges in the wire and cable industry, particularly for nuclear power generation facilities [20]. The 2024 rule extended the compliance deadline for processing and distributing decaBDE-containing wire and cable insulation until the end of the service life of these materials, recognizing the lack of fully qualified decaBDE-free alternatives meeting safety standards (such as IEEE Std. 383) and 10 CFR 50.49 requirements [20]. In addition, the EPA exposure assessment indicates that although releases of decaBDE could occur during cable manufacturing process, once formulated into the wire and cable, decaBDE is encased in the cured coating with minimal potential for worker exposure [20, 23].

1.4 Research Objectives

Since decaBDE has long been relied upon as a flame retardant in one of the most common XLPE nuclear cable insulation formulations, RSCC Firewall® III insulation, questions have naturally arisen regarding whether changes in cable performance might be expected for XLPE containing a decaBDE alternative, especially for safety-related cables that must perform their safety function in a design basis event such as a loss of coolant accident [24]. The research described here aims to directly investigate observable differences in material performance of the standard historical decaBDE-containing XLPE insulation and of the newly formulated XLPE containing a decaBDE alternative for samples subjected to accelerated thermal and gamma radiation aging. Mechanical properties, thermal oxidative resistance, chemical structures, and discoloration of XLPE samples provided by the manufacturer with and without decaBDE were determined after various thermal and radiation aging conditions. To quantitatively conclude whether a change in formulation caused different aging behaviors, statistical analyses were performed to test the difference between samples of the two formulations in their measured properties.

Finally, signature aging behaviors, called “knowledge gaps” in the Expanded Materials Degradation Assessment (EMDA) volume 5 [25], are briefly discussed with data obtained on this project.

2. EXPERIMENTAL

2.1 Materials

The two formulations, designated herein as XLPE-dBDE and XLPE-Alt, were provided for this study by RSCC. Over 400 ft of cable was supplied for each formulation. Insulated wires were received wound on spools, as shown in Figure 3. Information about the two cable samples used in this study is given in Table 3. The base polymer is XLPE.

Table 3. Information of cable insulations investigated.

Material ID	Contains decaBDE	Prints on insulation or jacket	Color	Release date
XLPE-dBDE	Yes	1/C 14 AWG COPPER RSCC XLPE KXL-760G DECABDE ZZU2301-001 2024	Natural	2023
XLPE-Alt	No	1/C 14 AWG COPPER RSCC XLPE KXL-760G NON-DECABDE ZZU2301-002 2024	Natural	2023

Figure 3. XLPE-dBDE cable insulation on a wooden spool.

The XLPE-based insulations from the same cable manufacture have been commercially available and have been supplied by RSCC and purchased for previous aging studies as a representative XLPE-based nuclear-grade cable insulation [26–28]. The estimated composition of the commercial XLPE-based insulation, as listed in Table 4, was determined using a combination of analytical techniques by Liu et al. [26, 27]. Approximately 10 wt.% of decaBDE was detected from the evolved products of pyrolysis of the commercial XLPE-based insulation [27]. Therefore, it was assumed that the XLPE-dBDE specimens used in this study had a similar composition to the commercial XLPE. It should be noted that the composition given in Table 4 was only deduced based on common additives in a cable for research purposes and was not confirmed by the cable manufacturer.

Table 4. Estimated composition of a commercial XLPE-based insulation [26, 27].

Component	Approximate weight ratio (%)	Function
Crosslinked polyethylene	60 ± 8	Polymer matrix
Decabromodiphenyl ether ($C_{12}Br_{10}O$)	10 ± 4	Flame retardants
Octabromodiphenyl ether ($C_{12}H_2Br_8O$)	10 ± 4	
Antimony trioxide (Sb_2O_3)	17	
Zinc sulfide (ZnS)		White pigment
Poly(1,2-dihydro-2,2,4-trimethylquinoline)	2	Antioxidant, metal deactivator
1,3,5-Triazine-2,4,6(1H,3H,5H)-trione	trace	Cross-linking booster

2.2 Sample Preparation

As-received insulation wires were sectioned into 120 mm long samples. For specimens prepared for thermal and mechanical testing, the metal conductors were removed prior to aging. Figure 4(a) shows the layout of the insulation stripping tool and the cables to be cut. A cable stripper (The Eraser Company, Inc, Model LSR10) was clamped to the bench with two C-clamps. Die blades of 0.079 in. (part # IR1707) were used based on the outer diameter of the insulation. The insulated wire from the spool was placed on the black movable platform, in between two rubber-covered clamps and through the hole in the die blade halves. As shown in Figure 4(b), when the handle was pulled, the blade halves closed, the platform moved in the same direction as the handle (downward in Figure 4(b)), and the cable clamps rotated in the opposite direction to secure the insulation as the insulation was pulled away from the blades (downward in Figure 4(b)). The insulation unwound from the spool was scored at the die blades, and the conductor wires were pulled from the scored location to leave the stripped insulation between the blade and the stopper, as shown in Figure 4(c). The length of samples was determined by the distance between the stopper and blade, which was set to 120 mm in this study, as shown in Figure 4(d).

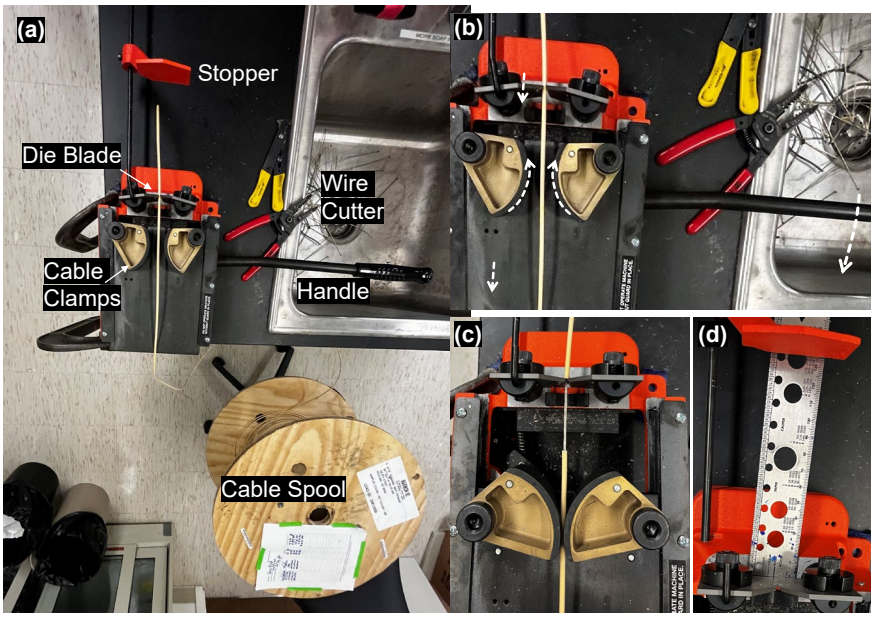

Figure 4. Stripping process to section insulated wires and to remove metal conductor from cable insulation.

2.3 Accelerated Aging

It has been a topic of interest in cable aging studies that the order of thermal and radiation aging can affect degradation pathways and the effects of insulation aging depend upon the material formulation and the metric of aging [25]. Specifically, the degree of degradation might be different if the same amount of thermal aging (the same duration at the same temperature) and radiation aging (the same duration, dose rate, and total dose) were applied sequentially (thermal followed by radiation, T→R), in the reverse order (radiation followed by thermal, R→T), or simultaneously (thermal and radiation applied concurrently, T&R). To thoroughly compare the aging behaviors of XLPE-dBDE and XLPE-Alt, all three combinations of aging sequence as well as the standalone thermal and standalone radiation aging conditions were carried out. The target number of aging days are listed in Table 5. At each time point, five insulation straws without metal conductors and three insulated wires with conductors were aged for each formulation.

Table 5. Accelerated aging program for XLPE-dBDE and XLPE-Alt specimens. (RT: room temperature).

Scenario	**T→R**	**R→T**	**T&R**	**T**	**R**
Specific conditions	150°C for *n* days, followed by 200 Gy/hr at RT for *n* days	200 Gy/hr at RT for *n* days, followed by 150°C for *n* days	150°C and 200 Gy/hr for *n* days	150°C for *n* days	200 Gy/hr at RT for *n* days
Target aging time, *n* (days)	0	0	0	0	0
	2	2	2	2	2
	4	4	4	4	4
	7	7	7	7	7
	14	14	14	14	14
	--	17	17	17	17
	21	21	21	21	21
	28	28	28	28	28
	--	31	31	31	31
	35	35	35	35	35
	39	39	39	39	39
	42	42	42	42	42
	46	46	46	46	46
	49	49	49	49	49
	53	53	53	53	53
	56	56	56	56	56
	60	60	60	60	60
	63	63	63	63	63

2.3.1 Thermal Aging

Figure 5(a) shows a photo of the aging ovens (Thermo Scientific, Heratherm OMH180) used for thermal aging periods. The oven temperatures were recorded using a datalogger (Omega RDXL6SD) connected with four K-type thermocouples, as shown in Figure 5(b). The probe end of thermocouples is indicated in Figure 5(c) with an arrow, measuring the temperatures slightly above and below the sample racks. The number in Figure 5(c) corresponds to the channel number in the datalogger. Each samples was cut to a 120 mm length and hung on a rack with an alligator clip one end of the specimen and a paper clip that connects the alligator clip to the rack, as shown in Figure 5(d). The racks were then placed into and taken out from the oven at target sample-switching dates. The replicates (five insulation straws and three insulated wires) removed from the oven were stored in an individual sample bag, as shown in Figure 5(e).

With the oven temperature set to 151°C, the actual temperatures were recorded by the datalogger every 5 mins. The temperature readings for the thermal-only aging (i.e., the "T" scenario in Table 5)

period are plotted in Figure 6. The measured temperatures were within the range of 149.8°C to 150.9°C. Brief temperature drops were caused by the opening of the oven door to retrieve the samples are each targeted time point. The temperature was stable throughout the entire aging period of 63 days. The difference in temperature between the four measured locations was less than 1°C, with the highest at the upper right side of the oven, as labeled with "1" in Figure 5(c), and the lowest at the lower left side labeled with "4 " in Figure 5(c).

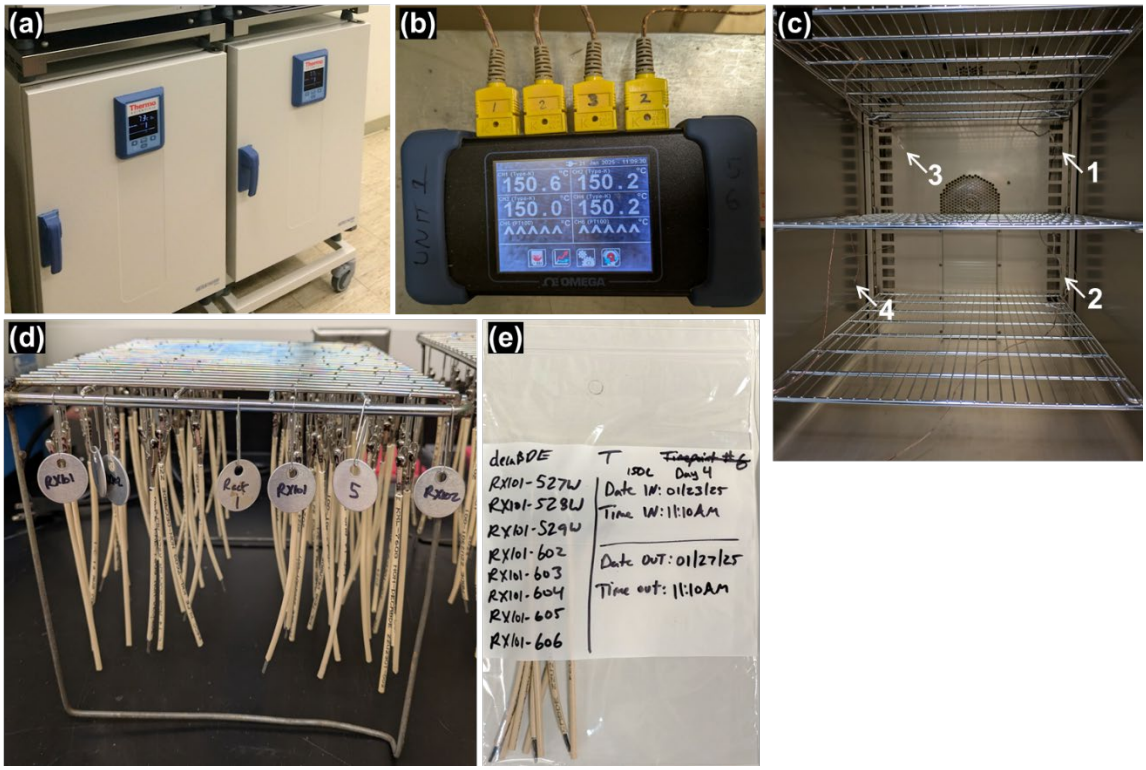

Figure 5. Thermal aging equipment: (a) oven, (b) temperature datalogger, (c) thermocouple locations. Specimens: (d) on a rack to be put into the oven, (e) in a sample bag for storage.

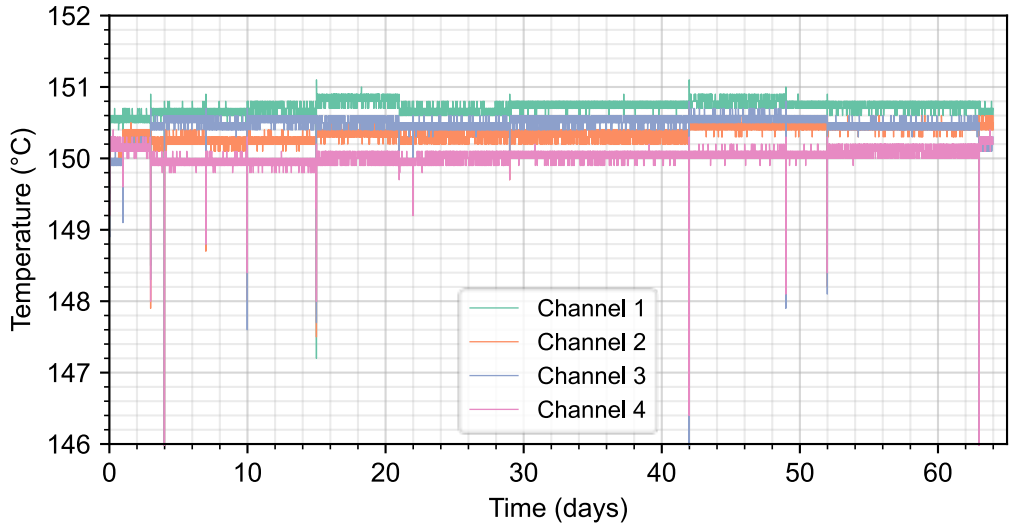

Figure 6. Temperature readings of four datalogger channels. The setpoint of the oven was 151°C. The "T" group specimens (requiring thermal-only aging) were placed inside the oven.

2.3.2 Radiation Aging

Radiation aging was performed in the High Exposure Facility (HEF) at Pacific Northwest National Laboratory (PNNL) in Richland, WA. A collimated gamma irradiator used ^{60}Co to expose materials to radiation at controlled dose rates [29]. Figure 7 shows the layout of the XLPE specimens hung on the racks facing the beam port. The specimens inside the oven were subjected to simultaneous aging ("T&R" condition in Table 5), while the specimens outside the oven at room temperature (RT) were subjected to radiation-only ("R" condition in Table 5) and to the radiation step in sequential aging scenarios ("T→R" and "R→T" conditions in Table 5). The RT radiation specimens were placed above, below, and on the left and right sides of the oven, as shown in Figure 8. The racks were slightly curved so that specimens were placed on an iso-dose-rate sphere. As shown in Figure 8, lead-based beam flattening filters were placed in between the specimens and the beam port for specimens whose distance to the beam port was closer than other specimens to offset the dose rates.

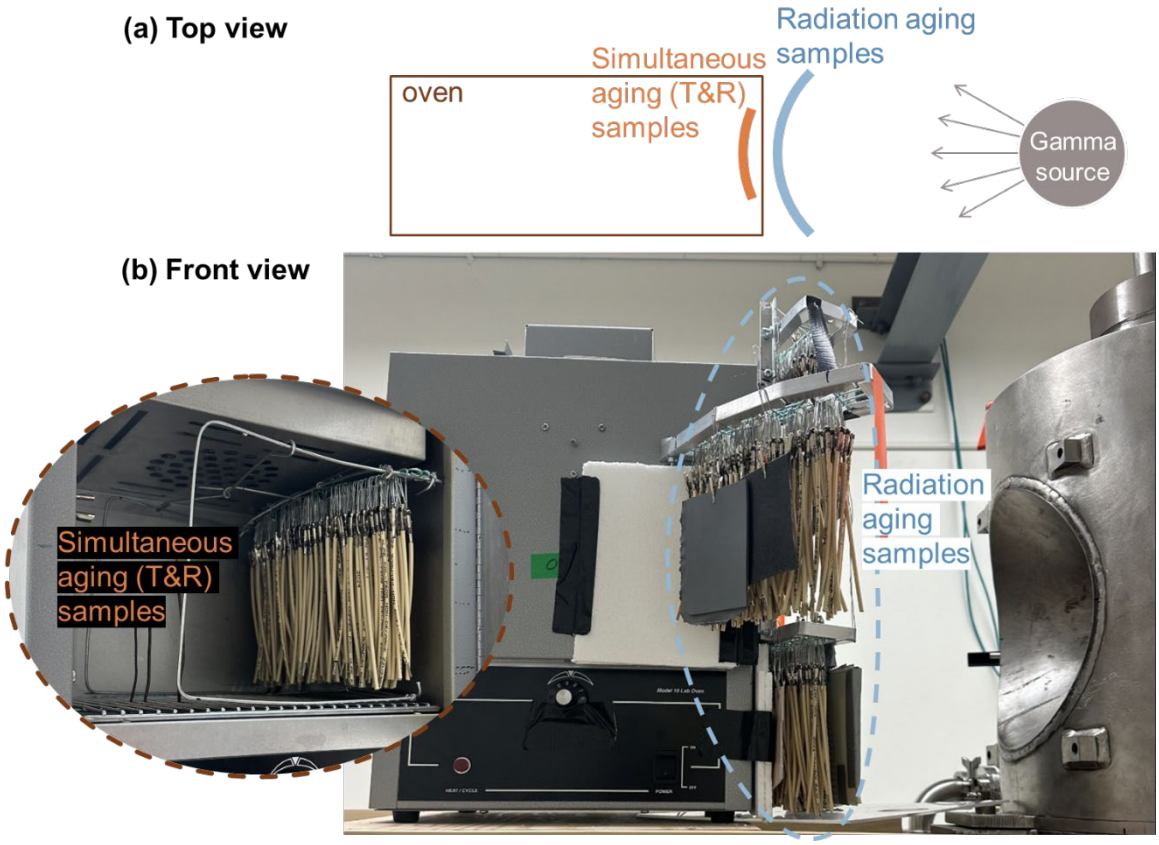

Figure 7. Layout of the cable insulation specimens in the High Exposure Facility (HEF) for gamma radiation aging. (a) top view showing the relative locations of the samples and irradiation source. (b) photos taken from the front, showing (left-most) samples inside an oven subjected to simultaneous aging, (middle) samples on the rack subjected to radiation aging at room temperature, and (right-most) irradiation column containing radiation source shielded by molten lead inside the column.

Figure 8. Arrangement of cable specimens subjected to radiation at room temperature, viewed from the side of radiation source (right view according to Figure 7a). The oven was behind the white insulation panel in the center. The lead-based beam flattening filters were added to attenuate the radiation received by cable specimens above and below the oven.

Dose rates at the different locations in the HEF assembly are given in Table 6. The dose rates at the middle row inside the oven and at the back rows outside the oven (above and below, left and right) were measured by a calibrated ionization chamber. Dose rates at other rows were calculated with respect to the measured rows using Equation (1), where R is dose rate, d is the distance to beam port, and subscripts denote two locations. Specimens at the front and back rows were switched halfway through the target aging time to achieve common average dose rates for specimens initially placed in different rows. The average dose rate was 194.42 ± 0.76 Gy/hr, as calculated by linear regression of accumulated dose as a function of aging time for all specimens. The accumulated total dose at 63 days was 28.75 Mrad (287.5 kGy). It should be noted that the XLPE-dBDE and XLPE-Alt samples of the same target aging time were placed in the same row and next to each other group, at which positions the dose rate was the same.

$$\frac{R_1}{R_2} = \frac{d_2^2}{d_1^2} \tag{1}$$

Table 6. Dose rate at the different locations near the radiation source. A darker background color indicates a higher dose rate.

	Dose rate (Gy/hr)		
Sample row	Inside oven	Above and below the oven	Left and right to the oven
Front	198.84	203.85	201.68
Middle	190.15*	No middle row	
Back	180.21	190.15*	190.15*

*Dose rate measured by a calibrated ionization chamber

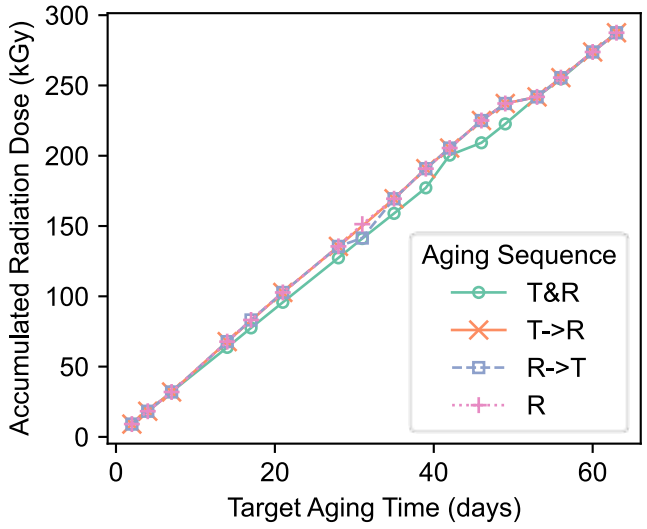

Figure 9. Actual accumulated total dose as a function of target aging time during the radiation aging step for specimens intended to be aged simultaneously (T&R), sequentially (T→R, R→T) and only under radiation (R).

2.4 EXPERIMENTAL CHARACTERIZATION

2.4.1 Yellowness Index (YI)

Yellowness index (YI) of insulation samples was measured for the unpigmented XLPE-dBDE and XLPE-Alt samples. Artificial daylight (CIE D65) illuminant was provided by a GTI MiniMatcher MM-2e viewing system. Background lighting in the room was extinguished during image collection. A Nikon D5300 camera was mounted on a tripod and oriented towards the display panel. To optimize the quality of the collected images, the digital camera settings used were as follows: an exposure time of 1/20 s to enhance color saturation, an aperture of f/5.6 to enhance depth of field, and an ISO speed of 100 to reduce background noise. Photos were taken using a wireless remote control (Nikon ML-L3) to avoid disruption to camera orientation. Three photos were taken for each specimen. The specimen was rotated and flipped between replicates to minimize deviation caused by differences in light condition and camera angle at different pixel positions within a frame.

Three photos were taken for each specimen. Eight specimens (including three with conductor and five without conductor) of each formulation (eight specimens of XLPE-dBDE and eight specimens of XLPE-Alt) were photographed, giving 24 replicates for every YI data point. Photos of select specimens, such as the unaged ones and the most aged ones (T&R, 63 days), were taken on different days after aging as a tracker for any reversible color change as well as a reference to ensure the same light conditions and camera settings. For example, a total of 47 replicate photos of the eight unaged XLPE-dBDE were recorded. YI was calculated using pixels within the region of interest (ROI), as shown in Figure 10. Only one YI value was obtained from each photo regardless of the number of ROIs defined.

Figure 10. Photo of an XLPE-Alt sample next to the color reference card for calibration. Yellow dotted line rectangle on the cable sample indicates the boundary of region of interest (ROI). Pixels within the ROI were used for YI calculation.

Due to their inherent components and internal processing, a digital camera and lens will modify the color in digital images; therefore, it is necessary to map these modified colors into a system with an absolute measure of color prior to quantifying color changes in specimens tested. As shown in Figure 10, an X-rite color checker containing 24 colors was placed next to the cable sample to fit in the same photo frame. National Institute of Health-developed ImageJ software was used in conjunction with the micaToolbox to convert the collected image values to CIE XYZ color space. First, the six grey standards located on the bottom row of the color reference target were converted to reflectance values using manufacturer-supplied standard Red Green Blue (sRGB) triplets for each grey standard and then using an iterative least log slope approach to convert the triplets to reflectance values. Second, the grey reflectance values were used to create a linear normalized reflectance stack, or calibrated multispectral image, for each collected image. Third, a cone-catch model was generated based upon the charted reflectance spectra of the color reference target. Lastly, the cone-catch model was used to map the linear normalized reflectance stack to the CIE XYZ color space. Per ASTM E313, calculation of YI for a D65 illuminant is shown in Equation (2), where X, Y, and Z are the evaluated XYZ tristimulus values of the specimen.

$$YI = 100\,(1.2985 \cdot X - 1.1335 \cdot Z)/Y \tag{2}$$

2.4.2 Fourier-Transform Infrared Spectroscopy

Fourier-Transform infrared spectroscopy (FTIR) was used to identify chemical changes in materials through the tracking of absorption intensities at characteristic wavenumbers. An FTIR instrument (Bruker Alpha II) equipped with an attenuated total reflection (ATR) attachment was used to measure the infrared absorbance spectra of the outer surfaces of samples, at three different locations for each sample. The aged samples were pre-conditioned in a controlled-environment chamber (Caron Model 7000-25) set to 23°C ± 2°C and 50% ± 10% relative humidity for at least 48 hours. For each spectrum, 64 scans were collected at a resolution at 4 cm^{-1} to minimize signal variation due to random noise. Three locations were tested for each specimen.

Carbonyl index (CI) was calculated using Equation (3), where A is the absorption peak height, C=O referring to the carbonyl peak in the range of 1710–1720 cm^{-1}, C-H being the hydrocarbon peak at 1463 cm^{-1}. Peak was determined using a Python function *scipy.signal.find_peaks* which finds the local maxima of at least 0.01 prominence. For the unaged specimens with no prominent C=O peaks, the maximum absorbance value at potential C=O peak locations (1712, 1714, 1716, 1718 cm^{-1}) was used.

$$CI = \frac{A_{C=O}}{A_{C-H}} \tag{3}$$

2.4.3 Mass Change

An analytical balance (Mettler Toledo XPR205, 0.01 mg resolution) was used to measure the mass of the insulation specimens before and after every step of aging. For sequential (T→R) and reserved (R→T) aging scenarios, three mass values were recorded for each specimen, the initial, intermediate, and final masses. Relative mass change (Δm) was calculated for specimens without metal conductors before aging, according to Equation (4) where m_0 is the initial mass and m is the current mass. Five specimens for each formulation were measured at each time point.

$$\Delta m = \frac{m - m_0}{m_0} \tag{4}$$

2.4.4 Oxidation Induction Time

Oxidation induction time (OIT) was measured following IEC 62582-4 on a differential scanning calorimeter (DSC Q2000, TA Instruments, see Figure 11) with the RSC90 cooling accessory. Calorimetry was calibrated per ASTM D4565 using indium and tin standards. A Tzero pan was used to contain a thin slice of the insulation sample of 5–10 mg. A pan lid was not used. The sample was heated in an N_2 atmosphere of 50 mL/min flow rate at a heating rate of 20°C/min up to 220°C. After stabilizing at 220°C for 5 min, the cover gas was switched to pure O_2. The temperature was kept at 220°C for a designated period, varying from 20 mins to 2 hrs, until an exothermic peak was observed.

Figure 11. Differential scanning calorimeter for Oxidation Induction Time testing.

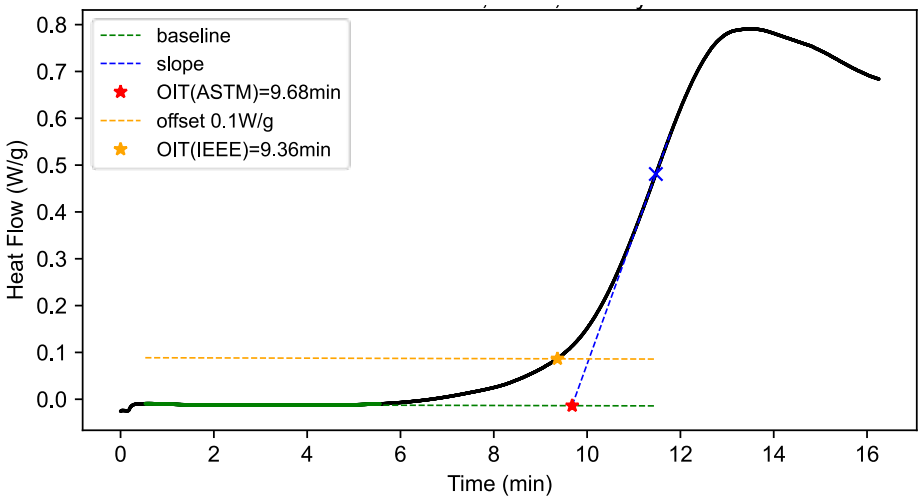

Figure 12. Determination of oxidation peak onset as the intersection (red star) of the baseline (green dashed) and the tangent line of the exothermic peak slope (blue dashed) as described in ASTM standards, and as the intersection (yellow star) of the shifted baseline (yellow dashed) and data curve (black solid) as described in IEEE/IEC 62582-4.

OIT refers to the time elapsed between switching on O_2 until the onset of the exothermic oxidation peak. The onset of the oxidation peak was defined differently in ASTM standards (D3895, D4565, E1858, D3350, D5885) and in IEEE/IEC 62582-4. As illustrated in Figure 12, ASTM standards specify the onset being the intersection of the baseline and the tangent line of the oxidation peak slope, while IEEE/IEC 62582-4 obtains the onset of oxidation by shifting up the baseline by 0.1 W/g to intersect with the signal trace. OIT reported in section 3.4 was determined following IEEE/IEC 62582-4.

2.4.5 Tensile Elongation at Break (EAB)

Uniaxial tensile testing, including EAB, was performed following IEC/IEEE 62582-3. After aging, the samples were pre-conditioned for 48 hours in an environmental chamber (Caron Model 7000-25) controlled at 23°C ± 2°C and 50% ± 10% relative humidity, per ASTM D618 Procedure A.

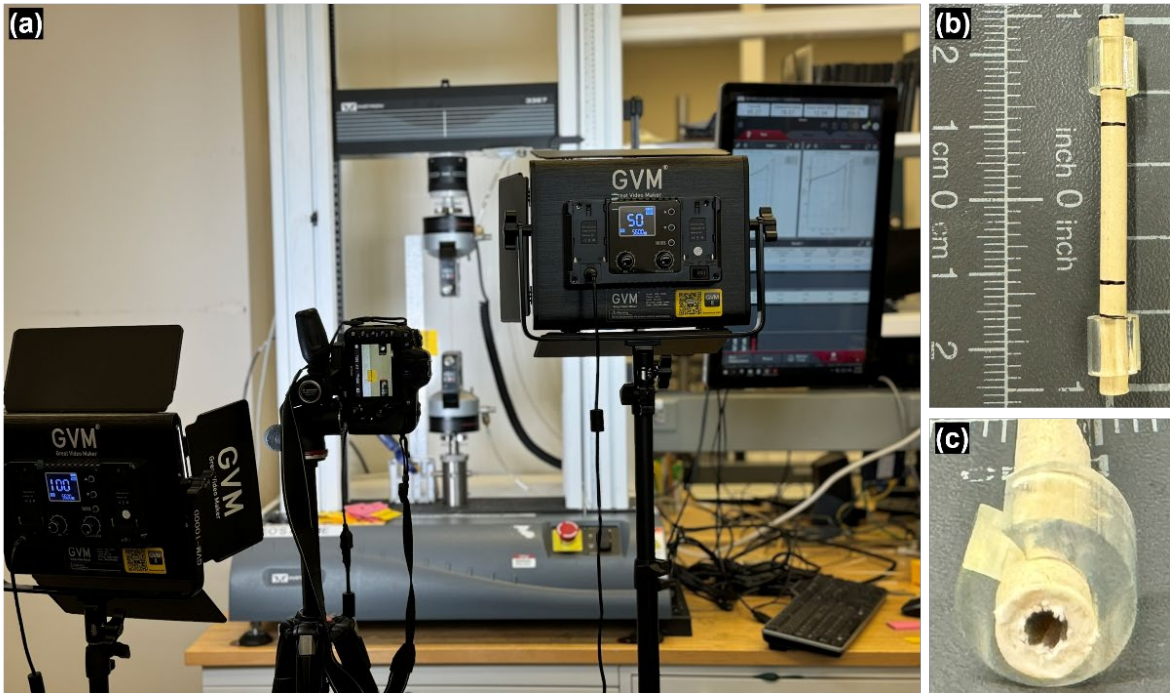

Figure 13. (a) Layout of the tensile testing setup. (b) Gauge marks on an XLPE-dBDE sample. (c) End tab of an XLPE-dBDE sample.

For tensile testing each sample was cut to 50 mm and loaded into an Instron 3360 test frame equipped with a 1 kN load cell and pneumatic grips. The grip pressure was set to 15–20 psi. As shown in Figure (c), end tabs were used to prevent slippage or crushing of the sample by grip pressure. The end tab was cut from a polyurethane tube into an approximately 8 mm length and was placed 1–2 mm from the sample ends. As shown in Figure (a), videos of sample breaking were recorded by a digital camera for strain calculation with home-built extensometer software. Gauge marks were drawn on samples to assist strain detection, as shown in Figure (b) where two black marks at 20 mm separation were drawn with an ultrafine permanent marker. The grip separation was 30 mm. A pull rate of 10 mm/min was used to minimize premature failures. Data points were not included if the samples did not break within the gauge section (such as at the grip).

2.5 Statistical Analysis

Statistical significance of mean differences between cable formulations was evaluated using two-sample Welch's t-tests. The t-test is a common statistical method for comparing means between two independent groups when the underlying population distributions are approximately normal. Given the small and sometimes unequal sample sizes, Welch's modification of the standard t-test was employed to accommodate unequal variances between the two cable formulations.

The null hypothesis (H_0) stated that there is no difference in mean values of the measured material properties between the two cable types ($\mu_1 = \mu_2$), while the alternative hypothesis (H_1) specified that a significant difference exists between the group means ($\mu_1 \neq \mu_2$). The null hypothesis was rejected when the calculated p-value was less than the predetermined significance level of $\alpha = 0.05$, indicating statistically significant differences between cable formulations at the 95% confidence level.

The degrees of freedom for Welch's t-test were calculated using the Welch-Satterthwaite equation, which provides a conservative approximation that is typically lower than the degrees of freedom used in Student's t-test. This conservative approach reduces the risk of Type I errors (false positives) by requiring stronger evidence to reject the null hypothesis, thereby providing more stringent statistical control when variance assumptions are uncertain.

3. CHARACTERIZATION RESULTS AND STATISTICAL COMPARISONS BETWEEN MEASURED PROPERTIES OF XLPE-DBDE AND THOSE OF XLPE-ALT

3.1 Yellowness Index

The unpigmented XLPE-dBDE and XLPE-Alt insulation sampless appeared off-white, slightly yellow-tinted, and ivory, as shown in Figure 15. The YI values of unaged XLPE-dBDE and XLPE-Alt are 55.0 ± 2.8 and 54.0 ± 1.5, respectively.

YI increased with aging time. As shown in Figure 14, the aging time dependence of YI was different under the five scenarios. YI increased fastest under the simultaneous aging condition (T&R), reaching 101.2 ± 3.3 for XLPE-dBDE and 98.9 ± 5.0 for XLPE-Alt after 63 days of aging. Under the sequential aging condition (T→R) and the thermal-only aging (T), the YI increased with aging time within the first 15–30 days and reached a plateau after which YI fluctuated around a saturation YI value. However, such a saturation in YI was not observed in the reversed sequential aging condition (R→T) within the investigated time. The YI of samples subjected to radiation-only aging only slightly increased by roughly 3 units after 63 days, up to 58.3 ± 1.8 for XLPE-dBDE) and 57.0 ± 1.1 for XLPE-Alt.

In all aging scenarios and at most time points, the average YI values of XLPE-dBDE were consistently higher than the average YI of XLPE-Alt, as shown in Figure 14.

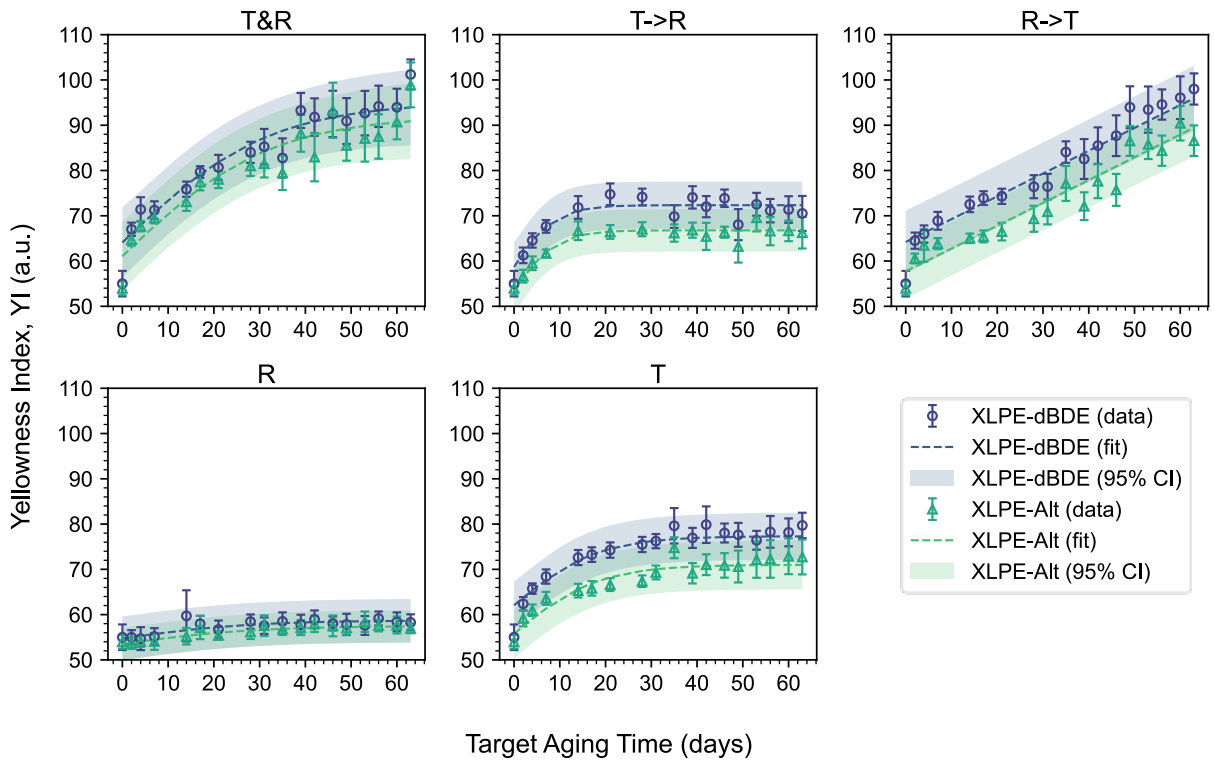

Figure 14. Yellowness index (YI) of XLPE-dBDE (blue circles) and XLPE-Alt (green triangles) aged up to 63 days at the five conditions listed in Table 5. Error bars represent standard deviation in test data. The aging condition was labeled in plot title. The dashed lines are fitting curves with fitting equations and parameters described in section 3.1.2.2. The shaded area represents 95% confidence intervals (95% CI) for the YI value predicted by the curve-fitting equations.

		Unaged	R 63 days	T->R 63 days	T 63 days	R->T 63 days	T&R 63 days
XLPE-dBDE	Photo	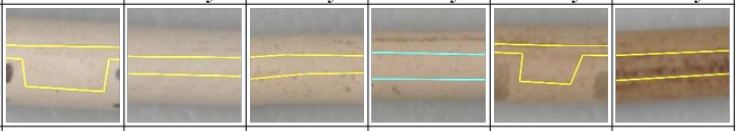					
	YI	55.07	58.29	70.47	79.88	97.69	101.28
XLPE-Alt	Photo	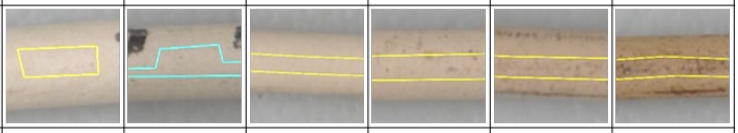					
	YI	53.97	56.96	66.07	72.87	86.84	98.97

Figure 15. Representative photos of cable insulation samples aged 63 days at five conditions compared to the unaged samples. The yellow and cyan lines represent the boundary of regions of interest (ROI). Pixels within ROI were used for YI calculation. The YI value associated with each photo is listed below the photo.

3.1.1 Potential Chemical Pathways

Referring to the insulation formulation components listed in Table 4, yellowing might be a combined result of polymer oxidation (as evident in FTIR spectra in section 3.2) and debromination and oxidation of the decaBDE and octaBDE components. The inorganic additives are typically stable at 150°C.

Carbonyl groups, as an oxidation product of XLPE, can act as chromophores and may contribute to the overall yellowing. In addition, the higher average YI of XLPE-dBDE compared to its dBDE-free alternative was perhaps associated with the discoloration induced by debromination of decaBDE compounds. Debromination can be initiated by ultraviolet (UV) light and result in the homolytic cleavage of C-Br bonds and generation of aryl and bromine radicals [30]. For the XLPE-dBDE aged in this study, debromination might happen with continuous heating. Although debromination through thermal degradation was generally observed above 500°C [31], the onset temperature can be lowered with the presence of: 1) a polymer matrix serving as a hydrogen donor that promotes hydrogenation/ debromination [32], 2) metal oxides such as antimony trioxide (Sb_2O_3) that catalyze the debromination reaction and may also catalyze the elimination of HBr/Br_2 in the condensation step (e.g., by formation of SbO_xBr_y) [33], and 3) polymer radicals initiated by polymer thermolysis or gamma irradiation. Radical-mediated chemistry not only furthers the debromination process that yields less-brominated diphenyl ethers, brominated dibenzofurans (BDFs), and brominated phenolic compounds, but also promotes oxidation reactions. The oxidized species are typically brominated phenols and can be quinone-like structures [34], which are known chromophores.

3.1.2 Statistical Analysis

To understand if the change in formulation from XLPE-dBDE to XLPE-Alt caused a statistically significant change in YI, two approaches were pursued: (1) directly comparing the mean YI difference of the two formulations using two-sample Welch's t-test with unequal variances, using the replicate YI data points at every aging level (every target aging time and condition); and (2) by first decomposing the effects of aging time and formulation using a curve-fitting model, and examining the effect of cable formulation with respect to measurement uncertainty. With both methods, the conclusions were consistent: a change in formulation from XLPE-dBDE to XLPE-Alt brings statistically detectable effects in YI under the sequential (T→R), reversed (R→T) and thermal-only (T) aging conditions, whereas the difference in YI under the other aging conditions including unaged, radiation only (R) and simultaneous (T&R), was not statistically significant.

3.1.2.1 Two-sample Welch's t-test with unequal variances

In the forest plot of t-test results in Figure 16, the null hypothesis is "no difference in mean YI between XLPE-dBDE and XLPE-Alt at the examined aging time and condition," i.e., $\langle \mathrm{YI(XLPE\text{-}dBDE)} \rangle - \langle \mathrm{YI(XLPE\text{-}Alt)} \rangle = 0$, with the angle brackets $\langle \mathrm{YI} \rangle$ denoting mean value. If the p-value is above 0.05 or the 95% confidence interval crosses 0, then the null hypothesis cannot be rejected, meaning there is insufficient evidence to conclude a significant difference in YI between the formulations under the investigated aging time and condition. Such a situation (i.e., $p>0.05$ and 95% CI interval crossing 0) was observed for the unaged specimen ($p = 0.46$), for six time points in T&R condition (7, 31, 35, 46, 60, 63 days), and most time points in R condition.

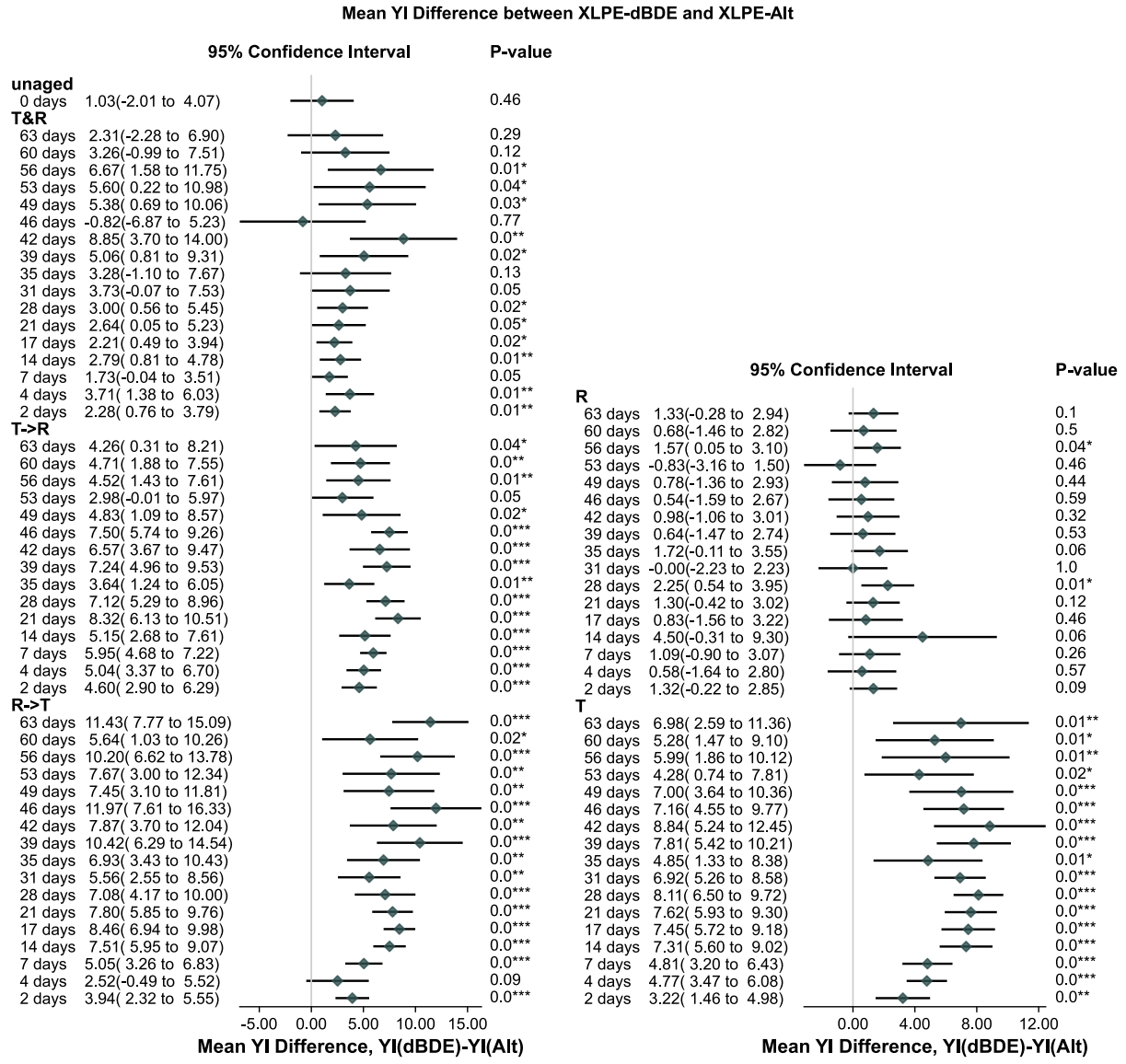

Figure 16. Forest plot showing the results of two-sample Welch's t-test with unequal variances, comparing the YI mean differences between XLPE-dBDE and XLPE-Alt, ⟨YI(XLPE-dBDE)⟩ − ⟨YI(XLPE-Alt)⟩, across target aging time up to 63 days and grouped by aging conditions. The green diamonds represent mean YI difference, where positive values indicate higher YI in XLPE-dBDE samples. The horizontal line represents 95% confidence intervals for the YI difference. The vertical gray line at 0 represents no difference between formulations. The p-values indicate the statistical significance of differences: $^{***}p<0.001$, $^{**}p<0.01$, $^{*}p<0.05$.

However, for the YI values at all except one aging time point under T→R and R→T conditions and all time points under T conditions, the p-values were below the significance level (0.05), and therefore the null hypothesis is rejected, meaning the difference in YI between the XLPE-dBDE group and XLPE-Alt group is statistically significant at the relevant aging times under T→R, R→T, and T conditions.

3.1.2.2 Deconvoluting aging and cable formulation effects

Since YI increased with aging time and saturated at a maximum value, a left-truncated sigmoid function was used to describe the aging time dependence [35]. The effect of cable formulation was assumed to be constant and not coupled with aging time (no interaction term).

$$YI = YI_0 + YI_{aging} + YI_{cable} = YI_0 + L \times \left[\frac{1}{1+e^{-kt}} - 0.5\right] + cable\_factor \times formulation \quad (5)$$

Equation (5) gives the assumed correlation between YI response, where YI_0 is the baseline and equals to the YI of unaged sample ($YI_0 = YI_{t=0}$) if the equation can perfectly fit data, and YI_{aging} and YI_{cable} are the decomposed terms accounting for the aging time (t) dependence and cable formulation ($formulation$) dependence respectively.

The aging time dependence was described by a left-truncated generalized logistic function ($L \times \left[\frac{1}{1+e^{-kt}} - 0.5\right]$). The -0.5 term shifts the curve to align its midpoint to day 0 and effectively truncated the left portion of the sigmoid curve. L is the amplitude of the sigmoidal curve and k represents the steepness of the upward portion of the sigmoid curve. Ideally, the amplitude L is the difference between YI baseline and the saturated YI due to aging, i.e., $L = YI_{t\to\infty} - YI_{t=0}$.

The "formulation" variable is assigned to 0 if the specimen is XLPE-dBDE and 1 for XLPE-Alt specimen. Therefore, the *cable_factor* is the constant that captures the difference in YI between XLPE-dBDE and XLPE-Alt.

Table 7. Optimized parameters to fit the YI responses using Equation (5) with a sigmoid aging time dependence, and the corresponding standard error and p-value for each parameter, and R^2 value denoting the overall fit quality. Shaded cells indicate overfitted results.

Set	parameter	optimized value	standard error	p-value	Note	R^2
T&R	*cable_factor*	-3.0241	1.1235	0.0112		0.8984
	amplitude	62.0777	5.0943	0.0000		
	steepness	0.0621	0.0101	0.0000		
	YI_0	64.0744	1.3144	0.0000		
T→R	*cable_factor*	-5.5575	0.4449	0.0000		0.9058
	amplitude	27.3179	1.4605	0.0000		
	steepness	0.2257	0.0210	0.0000		
	YI_0	58.6770	0.7471	0.0000		
R→T	cable_factor	-6.4915	0.8651	0.0000	Overfitted. No need to have all parameters.	0.9387
	amplitude	9.84E+03	4.64E+07	0.9998		
	steepness	0.0002	0.9674	0.9998		
	YI_0	64.2030	1.0134	0.0000		
R	*cable_factor*	-1.2408	0.1965	0.0000		0.7628
	amplitude	7.9643	0.5844	0.0000		
	steepness	0.0709	0.0125	0.0000		
	YI_0	54.7361	0.2805	0.0000		
T	*cable_factor*	-6.3080	0.5796	0.0000		0.9166
	amplitude	30.5151	1.6756	0.0000		
	steepness	0.1097	0.0147	0.0000		
	YI_0	62.0600	0.7920	0.0000		

The optimized parameters to fit the YI means using Equation (5) and the corresponding covariance matrix of parameters were given by a *scipy.optimize.curve_fit* function, where the weights were the reciprocal standard deviation of YI data. The parameters are given in Table 7. It was noticed that the p-

values for amplitude (L) and steepness (k) parameters when fitting the R→T set were almost 1, with the standard error being 3 to 4 orders of magnitude higher than the parameter value. This indicated over-parameterization in the aging time dependence portion. By checking the YI plot of R→T in Figure 14, the YI seems to be linearly correlated with the aging time and the saturation plateau was not reached yet. Accordingly, a linear aging time dependence instead of the generalized logistic function was used, giving the overall Equation (6) to fit the R→T data. The fitting parameters were given in Table 8, with no over-parameterization issue while maintaining a high R^2 value.

$$YI = YI_0 + YI_{aging} + YI_{cable} = YI_0 + \text{slope} \times t + cable\_factor \times formulation \quad (6)$$

Table 8. Optimized parameters to fit the YI responses using Equation (6) with a linear aging time dependence, the corresponding standard error and p-value for each parameter, and R^2 value denoting the overall fit quality.

Set	parameter	optimized value	standard error	p-value	R^2
R→T	*cable_factor*	-6.4915	0.8489	0.0000	0.9387
	slope	0.5041	0.0248	0.0000	
	YI_0	64.2030	0.8322	0.0000	

With the aging time and cable formulation effects decomposed in Equation (5) (or Equation (6) for R→T set), the effect of cable formulation is captured by the *cable_factor* parameter. Values of *cable_factor* are listed in Table 9. They are all negative, because the YI of XLPE-dBDE is higher than XLPE-Alt so that $cable\_factor = \frac{\partial YI}{\partial formulation} = \frac{YI(\text{XLPE-dBDE}) - YI(\text{XLPE-Alt})}{0-1} = \frac{a\ positive\ value}{-1} < 0$. Based on the p-values listed in Table 7 and Table 8 for *cable_factor*, which are all close to 0, this term cannot be reduced to capture the variations in data. However, the standard error and p-value for the *cable_factor* parameter in Table 7 and Table 8 only consider the "fitting uncertainty", and do not account for the uncertainty from the measurement. In addition, the R^2 values are not 1, meaning there is some amount of residual in data that was not captured by the fitting parameters. Therefore, the p-value associated with the *cable_factor* parameter alone does not tell if a change in formulation caused a statistically significant difference in YI.

A legitimate comparison is between the *cable_factor*, which reflects the effect of cable formulation captured by the curve-fitting model, and the pooled standard deviation of YI data ($\sqrt{\frac{\sum_1^n \text{data\_std}^2}{n}}$) reflecting the measurement uncertainty. A "signal-to-noise" ratio was calculated as $\text{Ratio} = \frac{\text{cable\_factor}}{\text{pooled\_std}}$ and given in Table 9. A ratio larger than 1 indicates that the effect of cable formulation outweighs the measurement uncertainty, as is listed in Table 9, for T→R, R→T, and T sets. Another justification for this conclusion is that the R^2 values are above 0.9, indicating that the fitting parameters could decently describe data, so that a *cable_factor* parameter can reasonably describe the effect of cable formulation in YI. The conclusion is consistent with that obtained from t-test in section 3.1.2.2.

Table 9. Effect of cable formulation described by *cable_factor* parameter in the curve-fitting models compared to the pooled standard deviation in measured YI data. Shading represents distinct behavior.

Set	Aging time dependence	*cable_factor* (effect of formulation)	Pooled standard deviation (measurement uncertainty)	Ratio
T&R	Sigmoid	-3.02	3.57	0.85
T→R	Sigmoid	-5.56	2.39	2.32
R→T	Linear	-6.49	3.10	2.10
R	Sigmoid	-1.24	2.07	0.60
T	Sigmoid	-6.31	2.52	2.50

3.2 Fourier-Transform Infrared Spectroscopy

FTIR detects changes in chemical structures of materials as a result of aging. Typically, oxidative aging of XLPE generates carbonyl groups that manifest as a peak in the 1700–1750 cm^{-1} wavenumber range, a strong indicator that tracks polyolefin oxidation. To understand the degradation status of the specimens, FTIR was performed for selected specimens. Specifically, for each formulation, one unaged specimen and one specimen aged for the longest time period (63 days) under each condition was tested. The choice of test specimens assumes that more variation in FTIR signals can be detected with longer days of aging, to serve the purpose of comparing the difference in chemical structural changes due to aging between cable formulations. The FTIR spectra for tested specimens are displayed in Figure 17 for XLPE-dBDE and in Figure 18 for XLPE-Alt. Prominent peak locations were labeled near each curve.

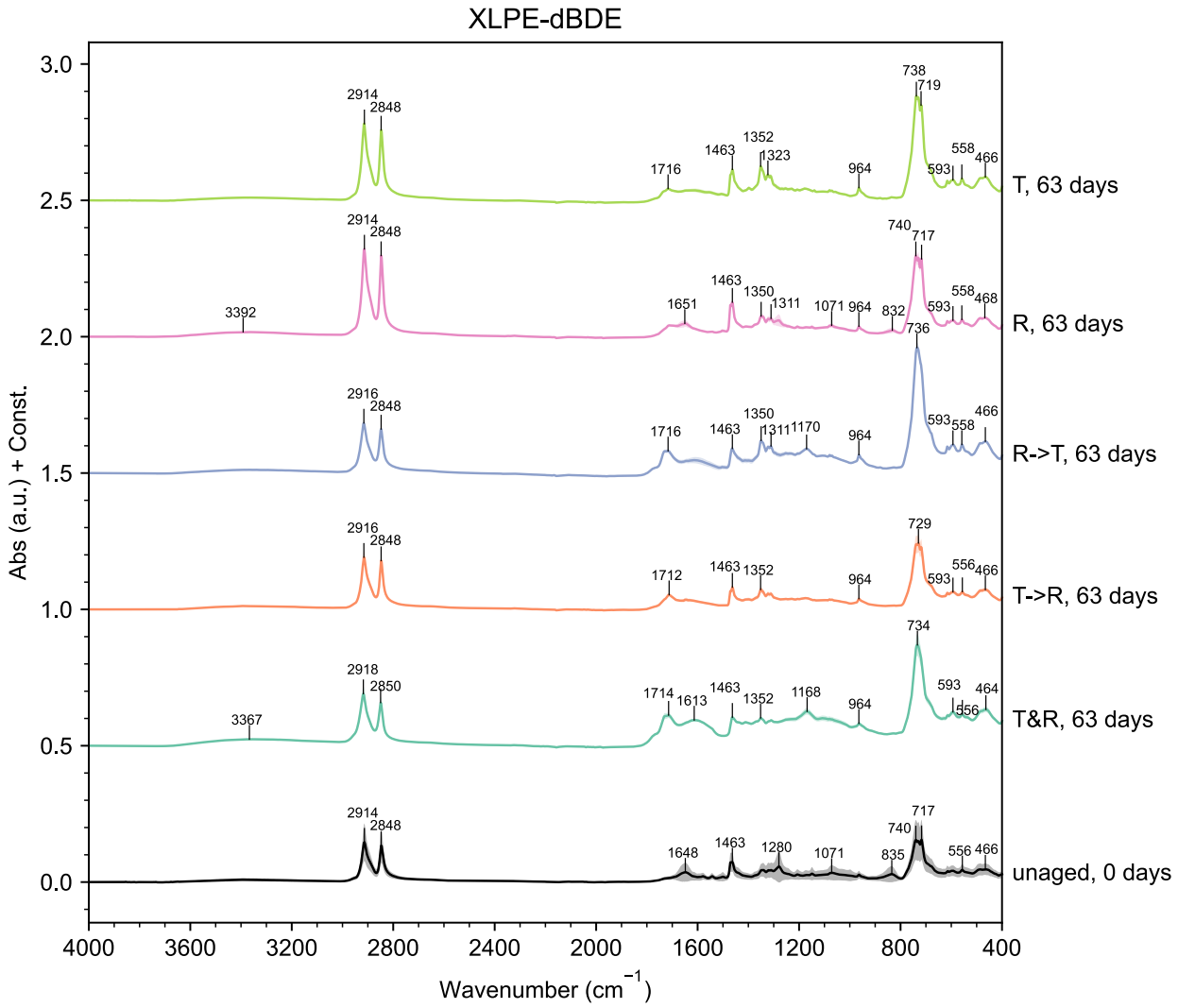

Figure 17. FTIR spectra of XLPE-dBDE samples aged for 63 days under the five conditions. The aging condition is labeled next to the spectrum. Curves are shifted vertically by 0.5 for clarity. The solid lines illustrate the mean values of FTIR absorbance averaged over three replicates, and the semi-transparent band indicates standard deviation. Wavenumbers (cm^{-1}) of prominent peaks are labeled above each curve. No spectra were normalized.

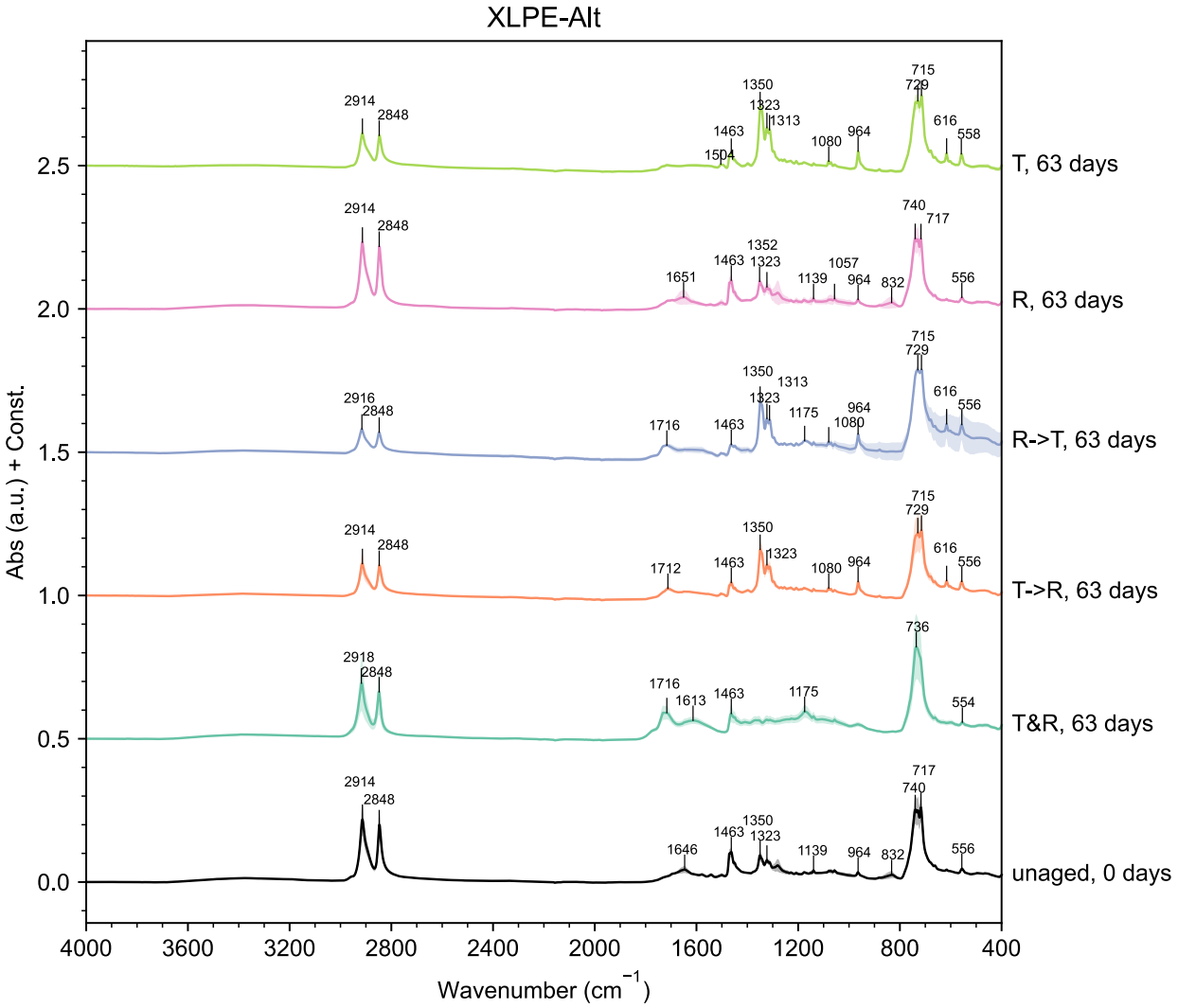

Figure 18. FTIR spectra of XLPE-Alt samples aged for 63 days under the five conditions. The aging condition is labeled next to the spectrum. Curves are shifted vertically by 0.5 a.u. for clarity. The solid lines illustrate the mean values of FTIR absorbance averaged over three replicates, and the semi-transparent band indicates standard deviations. Wavenumbers (cm^{-1}) of prominent peaks are labeled above each curve. No spectra were normalized.

Signature peaks for a pure polyethylene (PE) are listed in Table 10. In addition to the PE peaks, the unaged specimens showed additional peaks which are presumably associated with the additives in the cable insulation. Referring to the estimated components listed in Table 4, the peaks not associated with XLPE are listed in Table 11 with an estimation for the associated chemical structures.

Table 10. Absorption peak locations of a pure polyethylene.

Wavenumber (cm^{-1})	Vibrations
2914–2918	CH_2 asymmetric C-H stretching
2848–2850	CH_2 symmetric C-H stretching
1463	CH_2 scissoring
1350–1352	CH_2 wagging (small peak)
715–740	CH_2 rocking (two split peaks)

Table 11. Absorption peak locations in addition to those associated with PE and the speculated chemical structures.

Wavenumber (cm^{-1})	Estimation of associated chemical structure	Ref.
1648	C=O stretching in triazinone derivatives (residual of crosslinking booster) shifted due to polymer matrix	[36]
1280, 1313, 1323, 1350	C-O-C asymmetric stretching (connection between aromatic rings in BDE)	[37]
1070–1080	Aryl-Br valence from BDE	[37]
964	C-Br stretching in BDE	[37, 38]
556, 593, 616	Aromatic C-Br stretching in BDE	[37, 38]

As shown in Figure 17 and Figure 18, all aged specimens exhibit a peak in the range of 1712–1716 cm^{-1} (not labeled if the peak is mild) that is associated with the carbonyl (C=O) group, a signature oxidation product of XLPE. The most prominent C=O peak was observed in the T&R aging condition, followed by the R→T and T→R conditions. The C=O peak was normalized by the C-H scissoring peak at 1463 cm^{-1} to calculate the carbonyl index (CI), as shown in Figure 19. For the unaged specimens that do not show a carbonyl peak, the nonzero CI value was because the baseline was not perfectly flat due to an adjacent peak at 1648 cm^{-1}. The CI of radiation-only aged (R) specimens was only slightly higher than that of unaged specimens. The trend in CI was mostly consistent with the trend in YI results shown in Figure 15, except that CI of thermal-only aged (T) samples was lower than CI of T→R samples, while the reverse is true for the YI results. Since the carbonyl group is a chromophore, the consistency in the general trend makes sense, while the reserved order for T and T→R indicates that additional chromophores other than carbonyls were generated especially in thermal-only aging scenario.

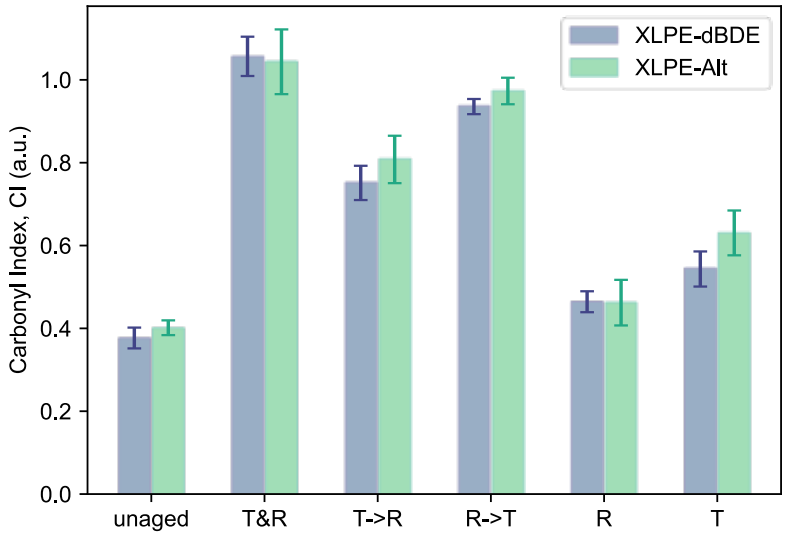

Figure 19. Carbonyl index (CI) of tested specimens calculated from FTIR spectra. Aging conditions are indicated in the x-axis label. Aging time was 63 days for all aging conditions.

3.2.1 Statistical Analysis

The two-sample Welch t-test with unequal variance was performed for the difference in CI values of XLPE-dBDE and XLPE-Alt reported in Figure 19. The 95% confidence interval and p-values are shown in Figure 20 for unaged and 63-day aged specimens under different aging sequences. Although the

difference in mean CI of XLPE-dBDE and XLPE-Alt are nonzero, the difference is not statistically significant.

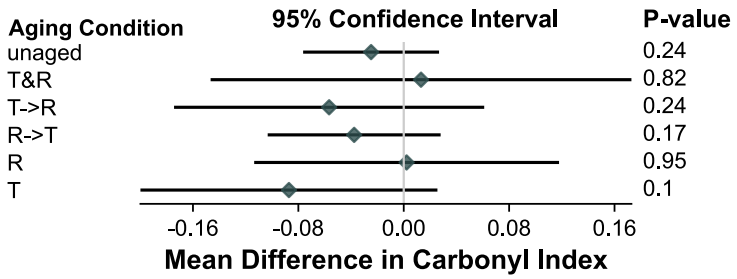

Figure 20. Forest plot showing the results of two-sample Welch's t-test with unequal variances, comparing the mean differences in carbonyl index (CI, as plotted in Figure 19) between XLPE-dBDE and XLPE-Alt, ⟨CI(XLPE-dBDE)⟩ − ⟨CI(XLPE-Alt)⟩, for unaged specimens and specimens aged for 63 days under five conditions. The green diamonds represent the mean CI difference. The horizontal line represents 95% confidence intervals for the CI difference. The vertical gray line at 0 represents no difference between formulations. The p-values indicate the statistical significance of differences.

3.2.2 Principal Component Analysis of FTIR Data

Although the carbonyl index often reflects the oxidative degradation status of polyolefin, it might not reflect the changes in other additives if their degradation products would cause FTIR signal variations outside the C=O or C-H ranges. Principal component analysis (PCA) is a more comprehensive dimension-reduction method that converts the multi-dimensional FTIR spectral data into several single-value parameters (i.e., principal component 1 or PC1, principal component 2 or PC2, etc.) while capturing most of the variation in data. It is a data-based approach that starts from phenomenologically summarizing the data and then correlating features in data to potential physical mechanisms. It serves as a complementary approach to the conventional, physics-based method, as has been pursued in the discussions around Figure 17, Figure 18, and Figure 19. It starts with chemical identification and then identifies the peaks that reflect changes in chemical structures based on the aging mechanisms (e.g., using carbonyl peaks to describe oxidative aging).

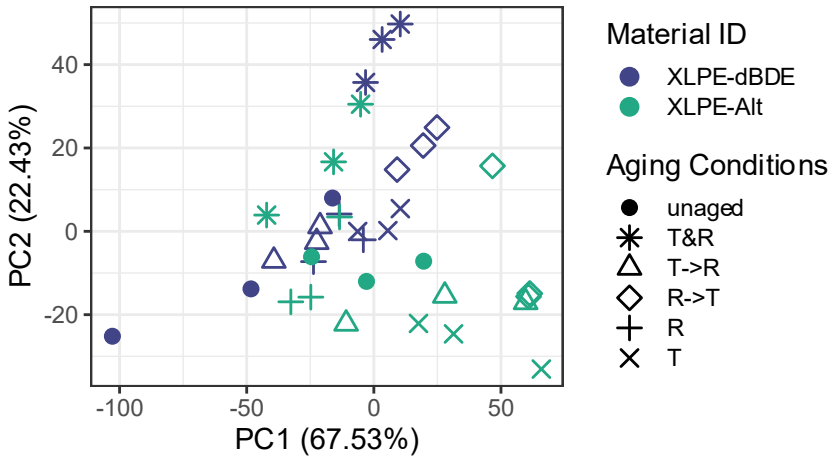

Figure 21. Principal component biplot of FTIR data of XLPE-dBDE (blue) and XLPE-Alt (green) specimens with different aging conditions (including unaged and 63-day aged with different thermal and radiation sequences) plotted in different symbols. Principal component 1 (PC1) accounted for 67.53% of variations in the FTIR data while principal component 2 (PC2) represented 22.43%.

The PCA results are shown in Figure 21 with the contributions to PC1 and PC2 plotted in Figure 22. Three replicate FTIR spectra were obtained under each aging condition, therefore three identical points can be observed. Both materials showed considerable variability among the three replicate points, indicating a large measurement uncertainty which may be related to material heterogeneity in samples within the same aging group. Despite the within-group variability, the XLPE-dBDE (blue) and XLPE-Alt (green) still occupied different PC spaces and showed distinguishable clustering patterns, indicating differences in FTIR response induced by differences in material formulation.

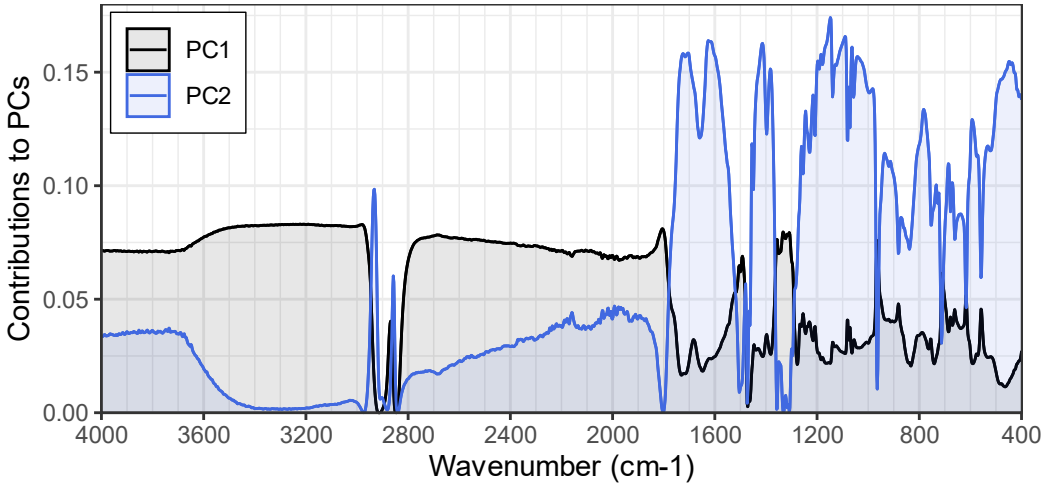

Figure 22. Contributions of variables to PC1 (black) and PC2 (blue). Contribution means the weight of the FTIR absorbance at each wavenumber when calculating PC1 and PC2 from each FTIR spectrum.

Across the aging conditions, the T&R points were the farthest away from the unaged points, indicating the strongest aging effects among the aging conditions investigated. For XLPE-dBDE, the T&R points shifted in the positive PC1 and PC2 direction, while for XLPE-Alt the T&R points shifted mostly in positive PC2 direction. The R→T points showed a different shifting direction away from unaged points compared to T&R points. The points in the other three aging conditions of XLPE-dBDE remained close to the unaged region. For XLPE-Alt, the T→R and T points showed negative PC2 shifts. The different shifting directions imply different chemical pathways of degradation.

The loading plots shown in Figure 22 demonstrate the contributions of spectral bands to PC1 and PC2 and reveal the chemical information captured by PC1 and PC2. The contributions to PC1 were relatively uniform across the entire wavenumber range, with higher weights given to the regions of lower FTIR absorbance signals. The PC2 loadings were more focused on the aging-related wavenumbers, with the highest contributions from the FTIR peak locations including 2800–3000 cm^{-1} and 400–1800 cm^{-1}. In general, the main difference in the loading profiles of PC1 and PC2 is that PC1 represents the overall differences between specimens while PC2 is more focused on aging-induced changes.

Because the (PC1, PC2) data points are two-dimensional with potential correlation between PC1 and PC2, the multivariate analysis of variance (MANOVA) method was used to test if the group centroids differ in the PC1-PC2 space between XLPE-dBDE and XLPE-Alt groups under each aging condition. The results are given in Table 12. Typically, if the replicate points are closer to each other (small within-group variance), and the points of XLPE-dBDE are farther away from the points of XLPE-Alt (large between-group distance) in the PC1-PC2 plot (Figure 21), it is more likely to exhibit statistically significant difference. Based on the p-values listed in Table 12, the XLPE-dBDE and XLPE-Alt specimens aged under T→R, R→T, and T conditions for 63 days showed statistically significant differences in their FTIR data. This conclusion is consistent with the statistical analysis results for YI data, as discussed in section 3.1.2. However, it should be noted that while the t-test can work reasonably well with small sample sizes, the MANOVA typically demands 10–15 replicates to gain the high degree

of freedom required by the F-distribution and to more robustly determine the covariance matrix. Therefore, even though the test being performed in PC1-PC2 space explained ~90% of variance in FTIR data, and the conclusion is consistent with that based on YI data, the statistical power is poor, and more replicates are needed to reach a robust conclusion with MANOVA.

Another metric to evaluate "closeness" between two formulations is the Wilks' lambda (Λ), which is calculated as the ratio of determinant of covariance matrix of data points within group to that of all data points. Therefore, a larger Λ (near 1) means more variances come from within the group and that the two groups being compared are less separated, while a smaller Λ (near 0) indicates that the formulation would show a larger effect on FTIR data. The Λ values as listed in Table 12 indicate that the two formulations subjected to radiation-only (R) are quite close (Λ=0.71), as can be visually observed in Figure 21. The results of XLPE-dBDE and XLPE-Alt specimens aged in sequential (T→R) and thermal-only (T) conditions are located at distinctly separated PC1-PC2 regions, as shown in Figure 21, and show the lowest Λ (0.04 and 0.05, respectively) as listed in Table 12. For the unaged and T&R groups, although the XLPE-dBDE and XLPE-Alt data show distinct separation, the within-group variance is also quite large, which gives moderate Λ values (0.31 and 0.19).

Table 12. Statistical analysis results on FTIR-derived PC1-PC2 data. MANOVA: multivariate analysis of variance. Wilks' lambda (Λ): proportion of total variance that is within groups. Λ→0: groups are completely difference. Λ→1: groups are identical. Shaded p-values indicate the statistical significance of differences: $^{**}p<0.01$, $^{*}p<0.05$.

Aging conditions	MANOVA on PC1-PC2	
	Wilks' lambda (Λ)	p-value
unaged	0.31	0.17
T&R	0.19	0.09
T→R	0.04	0.009**
R→T	0.11	0.03*
R	0.71	0.60
T	0.05	0.011*

3.3 Mass

Mass measurement is convenient and non-destructive. At certain aging periods for XLPE, mass change is roughly linearly correlated with aging time, under which conditions it can be used as a metric of aging. The relative mass changes in each aging condition are plotted in Figure 23. For the sequential (T→R) and reverse order (R→T) aging, intermediate mass was recorded so that the mass changes in the first and second stages can be calculated, as plotted in Figure 23. Comparing the mass changes in the two stages (the subplots in the second and third columns in Figure 23), the mass gain in the T→R condition mainly comes from its 2nd radiation-aging stage. for the R→T condition, although the 1st radiation-aging step caused a mass increase, this was subsequently offset by mass loss during the 2nd thermal-aging step. The two competing processes resulted in no apparent change in the R→T condition where mass seemed fluctuating around a constant value.

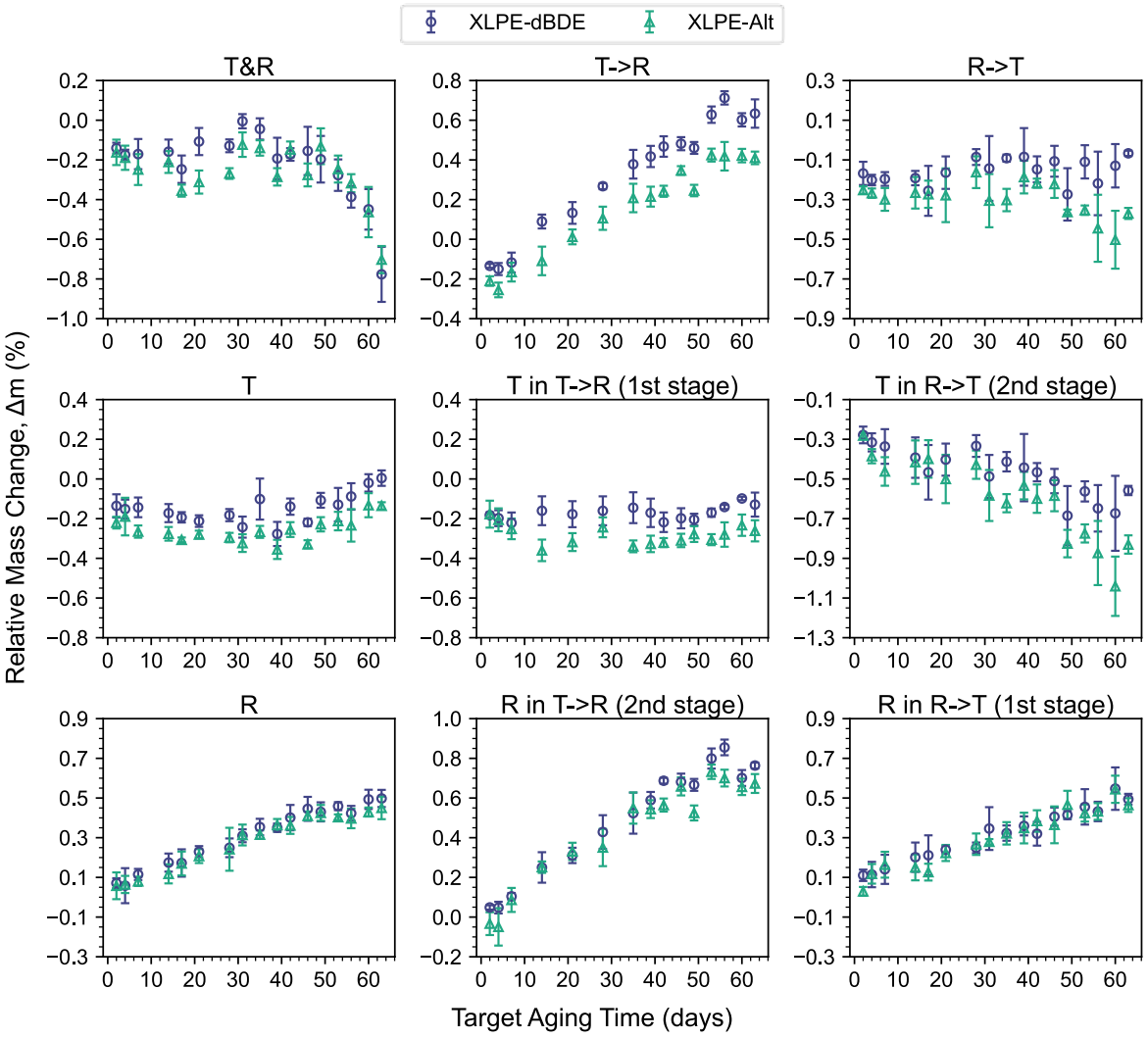

Figure 23. Relative mass change (Δm) of XLPE-dBDE (blue circles) and XLPE-Alt (green triangles) aged up to 63 days under the five conditions listed in Table 5 as well as under the individual stages in sequential (T→R) and reserved (R→T) aging conditions. Error bars represent standard deviation in test data. The aging condition is labeled in plot title.

In addition, by comparing the subplots in the last two rows in Figure 23, mass change during the 1st stage of T→R (the "T" stage) showed a very similar pattern as the mass change during the thermal-only aging (T condition), where the mass fluctuated in the range of -4% to 0% up to ~45 days and then increased with aging time. The similarity was also found for the mass change during the 1st stage of R→T and the radiation-only (R) condition, under which conditions the mass increased linearly with aging time up to ~5% in 63 days. These similarities were within expectations because the specimens being compared had no prior aging history and were subjected to identical conditions. However, mass change of specimens with aging histories showed different time-dependent trends. Mass decreased in the thermal aging stage if specimens had radiation aging history (2nd stage in R→T), as compared to almost no change in mass for specimens with no aging histories. As for the radiation aging, specimens with thermal aging histories (2nd stage in T→R) showed an increase in mass with roughly twice the aging rate of specimens without aging histories.

Under the simultaneous aging (T&R) condition, the mass of samples fluctuated in the range of -0.4% to 0% for the first ~45 days followed by a rapid decrease with aging time (from -2% to -8% in ~15 days).

Apparent synergistic effects were observed as the net effect of the superposition of thermal (T) and radiation (R) aging would be an increase in mass, which the simultaneous aging showed apparent decrease in mass.

The exact chemical pathways for mass gain and mass loss when not identified. However, the following degradation mechanisms might be relevant to the observed mass changes. First, it is reported for a commercially available XLPE-type cable that the antioxidant is effective in protecting the material from thermal aging but less effective in protecting the XLPE polymer from gamma radiation [39]. The depletion of antioxidants could explain the fluctuations in mass observed within a constant range for the first ~45 days of aging under the simultaneous (T&R) and thermal (T) aging conditions. Second, the mass gain during the radiation aging at room temperature (R condition and 1st stage of R→T condition) might be associated with rapid termination due to low mobility of radicals. Specifically, the role of gamma radiation is mainly to accelerate the initiation step (formation of radicals) of degradation, generating alkyl radicals (R·) [40]. In air, typically an alkyl radical reacts with O_2 to form a peroxyl radical (ROO·), which abstracts a hydrogen from another C-H bond to form a hydroperoxide (ROOH) and a new alkyl radical (R'·) [40,41]. The reaction between O_2 and alkyl radicals leads to a mass gain in the solid phase. Subsequently, the hydroperoxide breaks down quickly into alkoxyl and hydroxyl radicals, each of which can abstract a hydrogen to form new alkyl radicals, leaving a carbonyl group and H_2O [40,41]. Even with the removal of H_2O, the net mass change in the solid phase is still an increase since O_2 has a larger molar mass than H_2O. Under room temperature, chain mobility is very low in the crystal phase, therefore the new alkyl radicals are more likely to terminate by recombination than propagation. However, at elevated temperatures, radicals could propagate and transfer further and abstract additional volatile species such as additional H_2O, short-chain hydrocarbons (C_xH_y), CO, CO_2, ketones, aldehydes, carboxylic acids, etc., which could explain the net mass loss in the thermal-aging stage (2nd stage of R→T) and the simultaneous aging (T&R) condition. It is not clear why the mass began to increase in the thermal-only aging (T and the 1st stage of T→R) after ~45 days.

3.3.1 Statistical Analysis

The two-sample Welch's t-test with unequal variance was performed on mass change data of XLPE-dBDE and XLPE-Alt samples under different aging conditions and durations. As shown in Figure 24, difference in mass change between XLPE-dBDE and XLPE-Alt specimens after up to 63 days of aging is statistically significant under T→R and T conditions, as indicated by the near-zero p-values displayed in Figure 24 and by the fact that their 95% confidence intervals did not overlap zero.

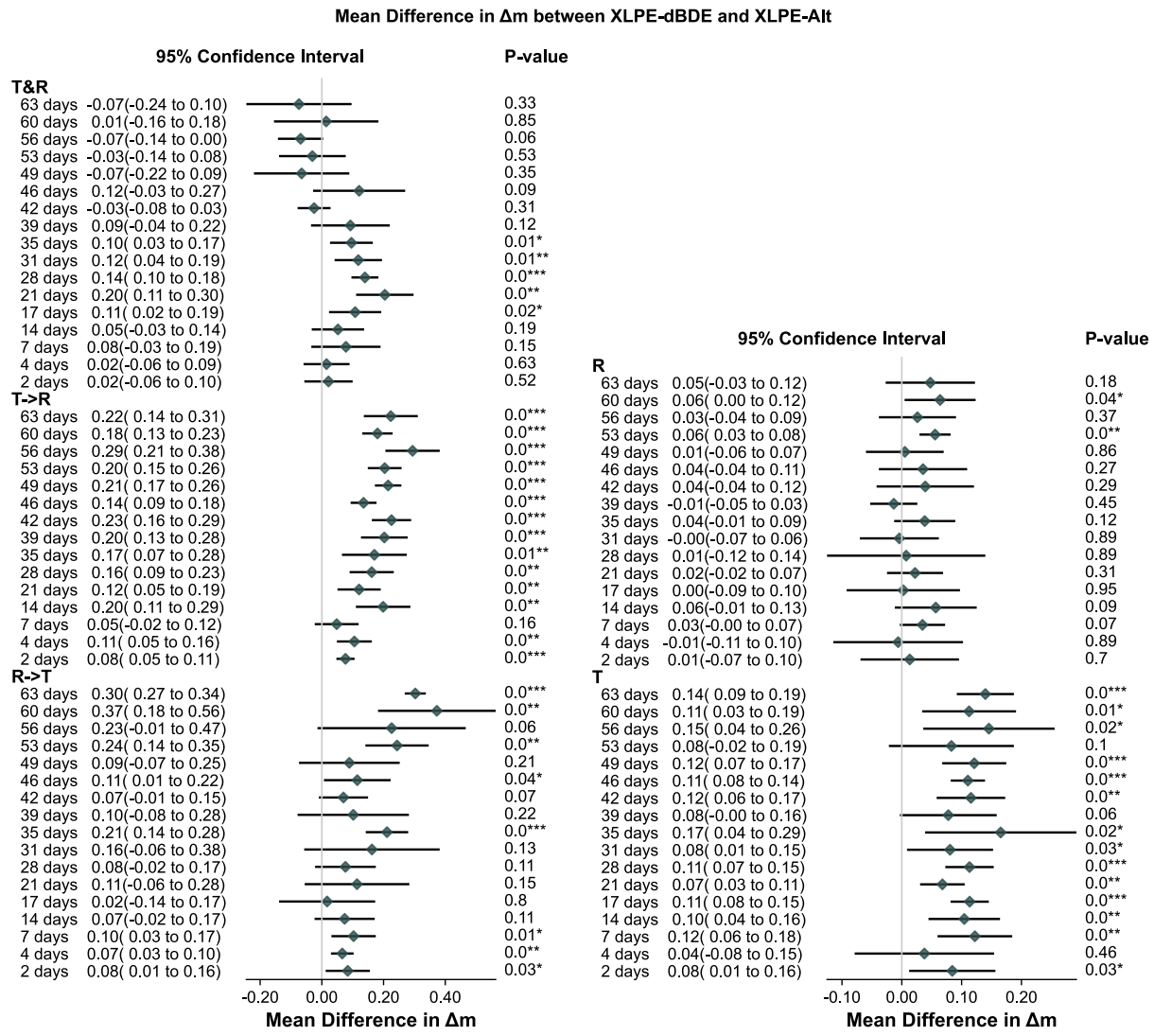

Figure 24. Forest plot showing the results of two-sample Welch's t-test with unequal variances, comparing the mean differences in relative mass change (Δm) between XLPE-dBDE and XLPE-Alt, $\langle \Delta m(\text{XLPE-dBDE}) \rangle - \langle \Delta m(\text{XLPE-Alt}) \rangle$, across target aging time up to 63 days and grouped by aging conditions. The green diamonds represents mean Δm differences, where positive values indicate higher Δm in XLPE-dBDE samples. The horizontal line represents 95% confidence intervals for the Δm difference. The vertical gray line at 0 represents no difference between formulations. The p-values indicate the statistical significance of differences: $^{***}p<0.001$, $^{**}p<0.01$, $^{*}p<0.05$.

3.4 Oxidation Induction Time

OIT is an empirical and direct measure of the time to consume all antioxidants in the oxidative environment at a high, degradative temperature, assuming that the antioxidants will be depleted before the exothermic polymer decomposition process initiates. Depletion of antioxidants does not cause immediate mechanical or dielectric failure of cable insulation but presages the degradation of the polymer matrix and loss of material elasticity. It should also be noted that OIT is not a direct measure of flame retardancy, although certain types of flame retardants can scavenge free radicals and increase OIT.

In this study, OIT was determined for XLPE-dBDE and XLPE-Alt samples exposed to pure oxygen at an isothermal temperature of 220°C. As shown in Figure 25, OIT decreased with aging time, which is within expectation as the antioxidants can be consumed during aging by the radical species. After 14 days of aging under T&R, T→R, and R→T conditions, OIT dropped to below 5 min, indicating complete depletion of antioxidants. Decrease in OIT under the thermal-only aging condition (T) was slightly slower than the combined aging conditions but still reached below 5 min after 17 days of aging. The antioxidants were effectively consumed under all of thermal aging conditions. As shown in Figure 25, the OIT decreased to 50–55 min after 39 days of radiation aging and remained unchanged up to 63 days.

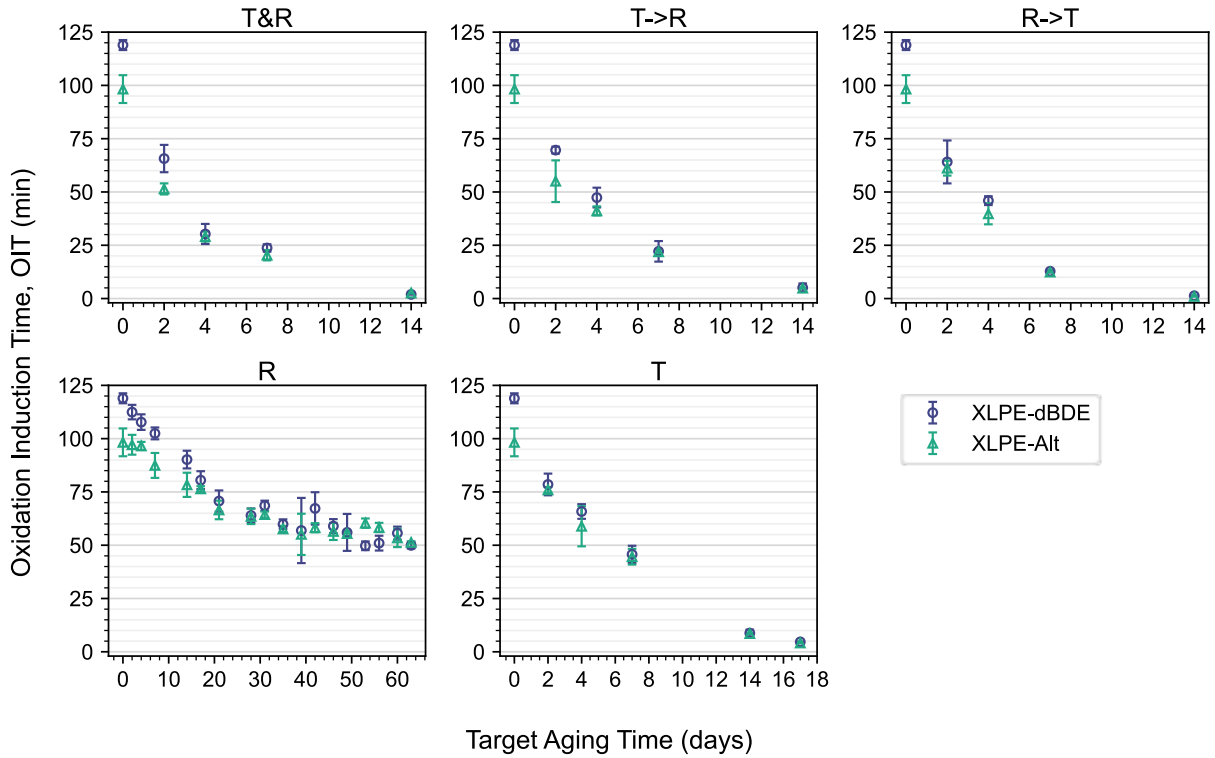

Figure 25. Oxidation induction time of XLPE-dBDE (blue circles) and XLPE-Alt (green triangles) aged up to 63 days at the radiation-only condition, 17 days at the thermal-only condition, and up to 14 days at the other conditions as listed in Table 5. Error bars represent standard deviation in test data. The aging condition is labeled in each subplot title.

3.4.1 Statistical Analysis

Comparing between the two formulations, XLPE-dBDE consistently showed higher OIT than XLPE-Alt, as shown in Figure 25 and Figure 26, although the difference in mean OIT values became smaller with the increase of aging time. The p-values listed in Figure 26 were below the significant level (0.05) for unaged specimens and the radiation-aged specimens within 7 days, indicating that there are

statistically detectable differences between the two formulations in terms of their thermal-oxidative resistance for fresh samples and for mildly aged samples before depletion of antioxidants. The differences in OIT became less pronounced as aging time increases. One possible explanation for the difference between formulations is that decaBDE could release bromide radicals to capture the other radicals generated in polymer molecules, thereby terminating the chain reaction, delaying the decomposition of polymers and increasing OIT. However, it should be clarified that antioxidant property (measured by OIT) and flame-retardant property (the primary function of decaBDE) are two different properties, which might be correlated but not interchangeable. The OIT results do not represent flame-retardant capabilities.

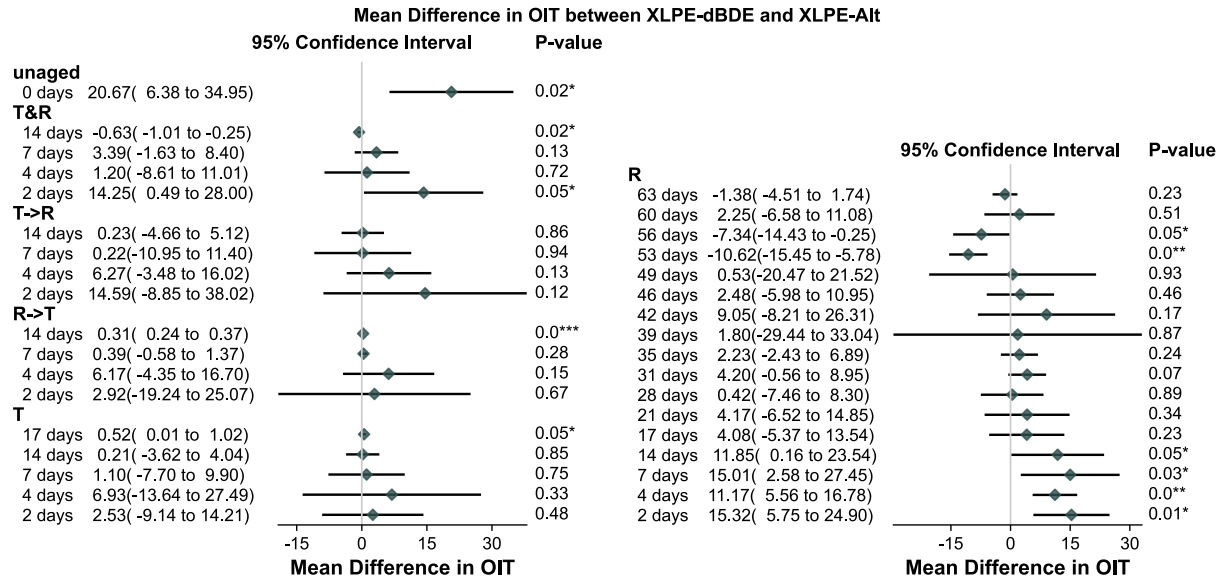

Figure 26. Forest plot showing the results of two-sample Welch's t-test with unequal variances, comparing the mean differences in oxidation induction time (OIT) between XLPE-dBDE and XLPE-Alt, $\langle OIT(\text{XLPE-dBDE})\rangle - \langle OIT(\text{XLPE-Alt})\rangle$, across target aging time up to 63 days at the radiation-only condition, 17 days at the thermal-only condition, and 14 days for other conditions, and grouped by aging conditions. The green diamonds represents mean differences of OIT, where positive values indicate higher OIT of XLPE-dBDE samples. The horizontal line represents 95% confidence intervals for the Δm difference. The vertical gray line at 0 represents no difference between formulations. The p-values indicate the statistical significance of differences: $^{***}p<0.001$, $^{**}p<0.01$, $^{*}p<0.05$.

3.5 Elongation at Break

Mechanical durability was quantified by tensile EAB. As shown in Figure 27, EAB slightly increased within the first 4–8 days for the samples aged under T&R, T→R and R→T conditions, followed by a rapid decrease with aging time. The T&R and T→R conditions are most degradative for the test specimens, where the EAB dropped to below 50% at around 40 days. The EAB of R→T samples dropped to around 100% at 40 days, being the least degradative among the sequential/simultaneous aging conditions.

The material degraded the slowest under the thermal-only aging condition (T). EAB showed an induction period of 30 days and dropped to around 90% EAB after 60 days of aging. The slow decrease in EAB under the thermal only condition is consistent with the mild mass change under thermal-only aging, and confirms that the material is thermally robust [39].

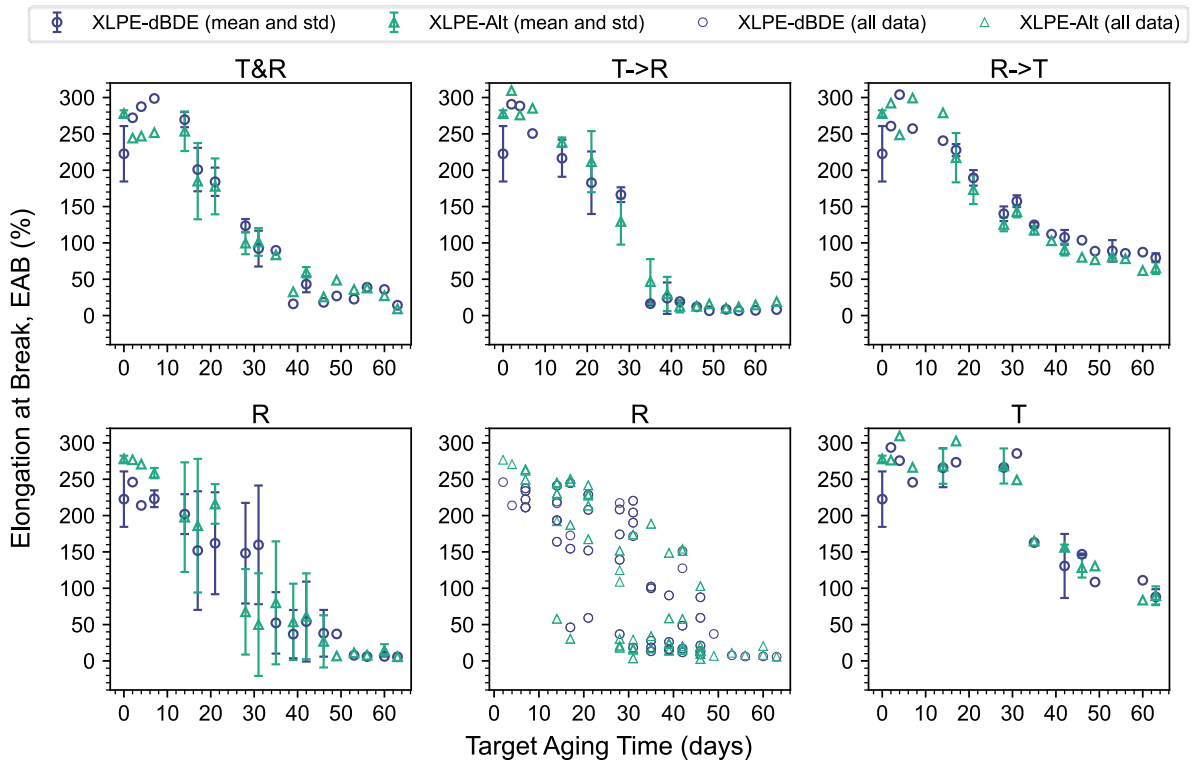

Figure 27. Elongation at break (EAB) of XLPE-dBDE (blue circles) and XLPE-Alt (green triangles) aged up to 63 days at the five conditions listed in Table 5. Error bars represent standard deviation in test data. The aging condition was labeled in plot title. The EAB values of specimens subjected to radiation-only (R) aging are plotted in two subfigures: one with mean and standard deviation (std) (left), and the other with all individual data points (center).

For radiation-only aged (R) samples, very large sample-to-sample variation is observed for specimens aged between 14 to 40 days. One specimen aged for 17 days dropped to below 50% EAB, lower than the T&R samples aged for 17 days (EAB ~200%). For the radiation-aged samples showing bimodal EAB trends, it was observed that the more ductile specimens (showing higher EAB) exhibited uniform strain distribution along sample length during the tensile test, whereas the specimens that broke at a low strain value showed localized necking and uneven strain distribution, as shown in Figure 28. The phenomenon that the radiation aged samples showed lower EAB at low temperatures compared to at high temperatures is called “inverse temperature effect”, and has been reported for some XLPE and EPR based samples [25]. However, other 17-day radiation-aged samples showed EAB above 150%, indicating that the inverse temperature effect can be sample-specific even for the same material. See Section 4.2 for further discussion.

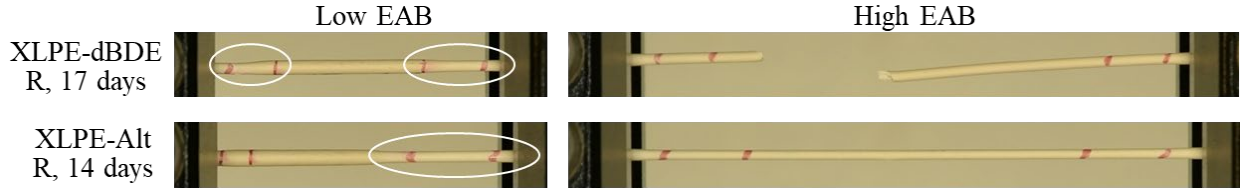

Figure 28. Photos of radiation aged specimens under tensile testing. Necking was observed in circled portions.

3.5.1 Statistical Analysis

Replicates were tested at the aging times where EAB dropped most rapidly. Differences in the mean EAB between XLPE-dBDE and XLPE-Alt are compared for the aging times where at least 2 replicates were tested, and the results are shown in Figure 29. At most aging levels, the differences in EAB between the two formulations is not statistically significant.

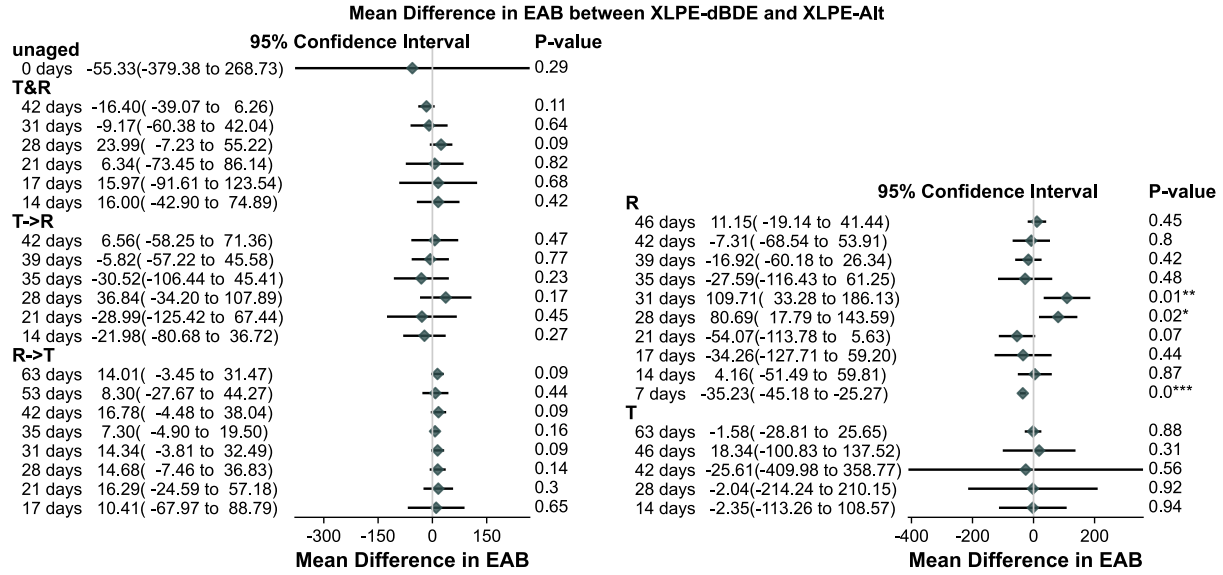

Figure 29. Forest plot showing the results of two-sample Welch's t-test with unequal variances, comparing the mean differences in EAB between XLPE-dBDE and XLPE-Alt, $\langle EAB(\text{XLPE-dBDE})\rangle - \langle EAB(\text{XLPE-Alt})\rangle$, across target aging times up to 63 days and grouped by aging conditions. The green diamonds represents mean EAB differences, where positive values indicate higher EAB in XLPE-dBDE samples. The horizontal line represents 95% confidence intervals for the EAB difference. The vertical gray line at 0 represents no difference between formulations. The p-values indicate the statistical significance of differences: $^{***}p<0.001$, $^{**}p<0.01$, $^{*}p<0.05$.

4. DISCUSSIONS

4.1 Sequential vs Concurrent Aging and Synergistic Effects

In IEC/IEEE 60780-323:2016, section 7.4.1.9.3, the aging conditions used in the cable qualification program are expected to "put the test sample in the worst state of degradation that it would experience during the qualified life." … "The sequence of age conditioning should consider sequential, simultaneous, and synergistic effects in order to achieve the worst state of degradation expected." However, there is little literature data directly comparing the severity of the three aging scenarios, i.e., simultaneous (T&R), sequential (T→R) and reversed (R→T). From the limited data listed in Table 13, the conclusions depend on polymer types and testing methods. In addition, the superposed effects of thermal-only aging and radiation-only aging (T+R) may be different from any of the sequential, reversed and simultaneous aging effects, exhibiting synergistic effects in the combined thermal and radiation aging conditions.

Table 13. Literature survey on relative severity of effect of sequence of thermal and radiation aging.

Base polymer, test	T&R	R→T	T→R	Reference
SiR, EAB	Most severe	Least severe of similar degree		[42]
EPR, EAB	Intermediate	Most severe	Least severe	[43]
EPDM, EAB	Intermediate	Most severe	Least severe	[28]
EPDM, FTIR	Most severe of similar degree		Least severe	[28]
EVA, EAB	N/A	Less severe	More severe	[44]
XLPE, EAB	Intermediate	Least severe	Most severe	[28]
XLPE, FTIR	Most severe	Least severe of similar degree		[28]
XLPE, EAB	Most severe of similar degree	Least severe	Most severe of similar degree	This work
XLPE, FTIR	Most severe	Intermediate	Least severe	This work
XLPE, YI	Most severe	Intermediate	Least severe	This work
XLPE, OIT	Not differentiable			This work

SiR: silicone rubber, EPR: ethylene propylene rubber, EPDM: ethylene propylene diene M-class rubber, EVA: ethylene-vinyl acetate, EAB: elongation at break, FTIR: Fourier transform infrared spectroscopy, YI: yellowness index

For XLPE-type cable insulation listed in Table 13, the carbonyl index as detected by FTIR increased most rapidly at the simultaneous condition (T&R), while mechanical degradation was the most severe in the T→R scenario—most probably related to the "inverse temperature effect" [28]. In the current study, the conclusion regarding EAB is different from the literature data. The T→R that was considered the most degradative scenario in literature showed similar severity to the T&R condition, indicating that the effect of ITE was not as pronounced for the samples used in this study. For CI measured by FTIR, the conclusion is the same that T&R represents the most degradative condition. YI showed the same trend as CI. OIT did not show any difference between the sequential and simultaneous aging conditions.

The severity in mass change is not directly comparable since mass increased under T→R condition but decreased under T&R and R→T conditions, as shown in Figure 30. The difference between mass gain and mass loss is related to different aging mechanisms as discussed in Section 3.3. The relative mass change under the standalone thermal (T) and radiation (R) aging conditions are added and plotted as "T+R" in Figure 30. The "T+R" data was not directly measured by experiments but represents the ideal condition if the thermal and radiation aging effects are independent and additive to get the combined effects (no synergistic effect). However, the T+R curve does not overlap with any experimentally obtained curves, indicating the existence of a synergistic effect. The synergism between thermal and radiation stress is potentially related to the degradation mechanisms involved: radiation accelerates radical generation, which is the rate-determining step in thermal aging, while heat enhances chain mobility and accelerates the overall depolymerization rates.

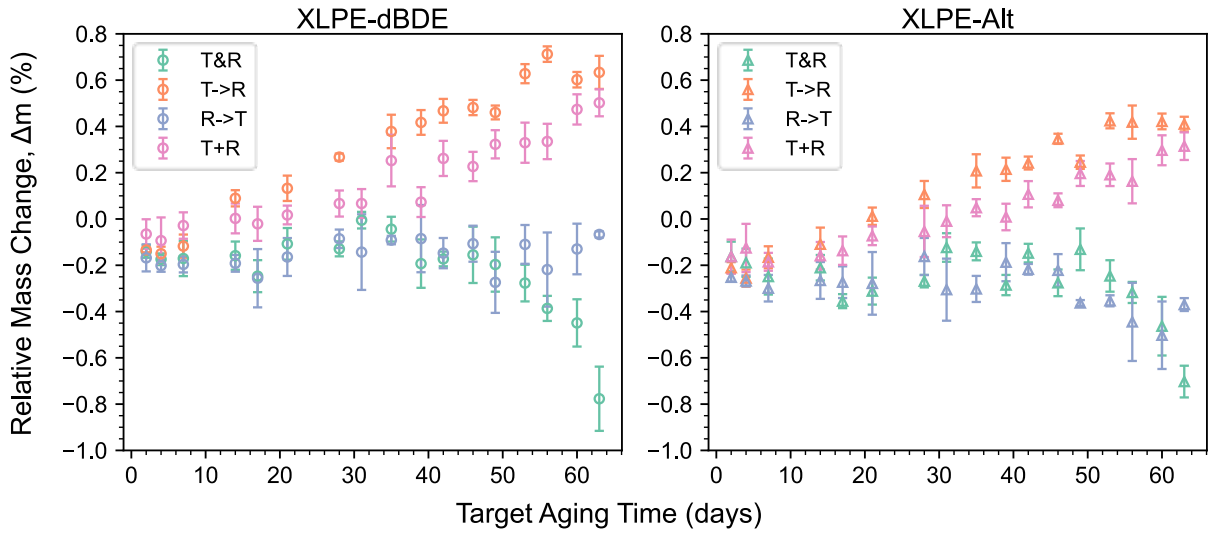

Figure 30. Relative mass change Δm (%) as a function of aging time for the different combinations of thermal and radiation aging: simultaneous (T&R), sequential (T→R), reversed order (R→T), and separately aged then superposed (T+R).

4.2 Inverse Temperature Effects

Inverse temperature effects (ITE) refers to the counter intuitive phenomenon in which degradation in the presence of radiation stress occurs more rapidly at lower temperatures than at higher temperatures. Not all XLPE- and EPR-based cable insulation materials exhibit faster decrease in EAB at lower aging temperatures. The phenomenon was believed to be related to low molecular mobility at low temperature, while the radicals generated by radiation caused chain scission and chemi-crystallization at the broken chain ends, inducing mechanical embrittlement. For the XLPE materials investigated, both formulations showed ITE under radiation aging at room temperature. However, the EAB data as plotted in Figure 27 clearly exhibited two branches, one branch showing ITE where the EAB decreased to below 50% after 17 days of aging, whereas the data on the other branch did not show ITE. The EAB on the non-ITE branch dropped to below 50% at around 49 days, which is longer than that under T&R condition (39 days).

The fact that some specimens showed ITE while others did not is consistent with the molecular mechanisms for ITE, as the embrittlement due to re-crystallization can be very localized. The site where thick crystals formed might experience stress concentration and initiate breakage upon stretching in the tensile test. Different components in the formulation also add to material heterogeneity. Inclusions and particles can also become defects for crack initiation.

5. CONCLUSIONS

Decabromodiphenyl ether (decaBDE) has historically been used in the formulation of RSCC Firewall® III crosslinked polyethylene (XLPE) insulation in cables and other environmentally qualified (EQ) components commonly present in U.S. nuclear power plants. The EPA has moved to ban decaBDE due to its persistent, bioaccumulative, and toxic (PBT) characteristics. RSCC has updated its XLPE formulation to one that does not include decaBDE. Cables and components containing the new XLPE formulation are available to nuclear customers, but awareness of this change in the insulation formulation prompted significant interest from the community regarding the equivalency of the new version to the old. XLPE-containing EQ cables may be exposed to thermal and gamma radiation stress in their service

environment and must be able to successfully perform their safety-related function following design basis events (DBEs). The standard qualification process involved thermally aging cables to the equivalent of 40 years of service using an Arrhenius methodology, exposing the cable to conservative 40 year gamma dose of 50 Mrad (500 kGy) and then subjecting the cable to a loss of coolant (LOCA) accident simulation involving a 200 Mrad (2000 kGy) accident dose and a scenario involve temperature and pressure swing, chemical spray, etc.

Direct comparison of decaBDE-containing XLPE and XLPE containing the decaBDE alternative in a complete EQ process including DBE simulation is beyond the scope of this work. However, investigation of combined effects of thermal aging and gamma radiation aging on the performance of the XLPE cable insulation formulation containing the standard historically used flame retardant component decaBDE versus those of the replacement XLPE cable insulation formulation containing the new decaBDE-alternative are interest to the nuclear community due to use of the material in safety-related applications and so laboratory investigation to directly compare these effects on the two materials was pursued. A total gamma dose of 30 Mrad (300 kGy) was targeted as relevant to actual exposure during 40 to 80 years of reactor service. A relatively high aging temperature was targeted to explore the complete degradation life of the thermally resistant XLPE cable (EAB degradation to less than 50%) in a manageable project timeline, acknowledging that accelerated aging artifacts such as diffusion limited oxidation may be present. Similarly, a dose rate of 200 Gy/h was targeted as a feasible way to reach 300 kGy total dose in reasonable project time while acknowledging that dose rate effects at this dose rate may be possible. The central objective was to directly compare the performance of the two XLPE formulations in a manner that challenges their thermal and radiation resistance rather than to precisely replicate aging in a specific plant environment over a specific period of service life.

XLPE-type cable insulation containing decaBDE (XLPE-dBDE) and XLPE containing a non-decaBDE alternative (XLPE-Alt), provided by the manufacturer in matching insulated conductor forms, were aged under five scenarios for up to 63 days of aging: thermal aging only (T), radiation aging only (R), simultaneous thermal and radiation aging (T&R), sequential aging of thermal followed by radiation (T→R), and sequential aging in the reversed order of radiation followed by thermal aging (R→T). The temperature used for thermal aging was 150°C. The radiation dose rate varies from 180.21 to 203.85 Gy/hr, depending on the location. The average dose rate was 194.42 Gy/hr, and the total accumulated dose was 28.75 Mrad at 63 days.

Material characteristics of XLPE-dBDE and XLPE-Alt insulations were compared in terms of color change using yellowness index (YI), chemical structural changes through FTIR especially carbonyl index, balance of material through mass change, antioxidant level through oxidation induction time (OIT), and mechanical performance through tensile elongation at break (EAB). Two-sample Welch's t-test with unequal variance was performed on the measured properties at each aging time under the five different conditions, to test if the differences between the average values of the two formulations were statistically significant considering the uncertainties in data curation. The results are summarized in Table 14. Statistically significant differences were found for specimens aged under sequential aging and thermal-only aging conditions using specific metrics such as yellowing, FTIR response, and mass change. The OIT of unaged samples was different between formulations but the difference became less pronounced and not statistically significant as the aging time increased.

Table 14. T-test results comparing the differences in material properties between XLPE-dBDE and XLPE-Alt specimens unaged and aged under different scenarios. Shades boxes indicate significance.

Metric	Unaged	T&R	T→R	R→T	T	R
Yellowness Index	n.s.	n.s.	*	*	*	n.s.
Carbonyl Index	n.s.	n.s.	n.s.	n.s.	n.s.	n.s.
FTIR PC1-PC2	n.s.	n.s.	*	*	*	n.s.
Relative mass change	--	n.s.	*	n.s.	*	n.s.
Oxidation induction time	*	n.s.	n.s.	n.s.	n.s.	n.s.
Elongation at break	n.s.	n.s.	n.s.	n.s.	n.s.	n.s.
*: Statistically significant difference was detected n.s.: No statistically significant difference, --: not applicable						

Both formulations showed different aging behaviors under thermal vs. radiation aging and the combined aging of different orders.

- Based on the OIT results, the antioxidant was not as effectively consumed under radiation-only aging as under thermal aging stages. The difference in the effectiveness of antioxidants between different aging conditions might explain why the relative mass did not change under the thermal aging or T&R conditions up to ~40 days but showed instantaneous mass gain under radiation aging. Another relevant observation is that the EAB decreased with aging time at the slowest speed under thermal-only aging, indicating the antioxidants are effective in protecting the materials from thermal aging.
- The decrease in EAB under radiation-only aging showed bifurcating trends at intermediate aging times (14 to 40 days, 6.5 to 20 Mrad), where some samples were much more brittle (EAB < 50%) than other samples (EAB in the range of 250% to 100% depending on aging time) aged for the same time. Necking was observed during the tensile test for the brittle samples, whereas the ductile samples showed uniform distribution of strain along the length. The embrittlement of certain XLPE and EPR type insulations under radiation at low temperatures has been recognized as an "inverse temperature effect" (ITE) in the cable community. The observed bifurcation in EAB trends indicates that even if the material is susceptible to ITE, it does not mean that all insulations made from the material will show ITE. The ITE being highly localized is consistent with the proposed mechanism related to the thickening of crystals at the polymer chain ends subjected to chain scission during aging.
- In addition to formation of carbonyl structures, a known chromophore for yellowing, the debromination of decaBDE might contribute to discoloration and explain the higher YI of XLPE-dBDE compared to XLPE-Alt.
- Among the three combined thermal and radiation aging conditions (T&R, T→R, R→T), simultaneous aging (T&R) was the most degradative for the specimens investigated. The superposed mass change by simply adding the mass change during standalone thermal (T) and radiation (R) aging conditions did not match any of the three combined aging conditions, indicating the synergism between heat and radiation mutually accelerates the degradation.

Statistical differences in aging behavior were observed between the two XLPE formulations in terms of color change, chemical bonding, and mass change. Antioxidant behavior differences were observed in the as-received formulations, but differences went away with aging. These observed differences are consistent with the fact that the XLPE-dBDE and the XLPE-Alt materials have different chemical compositions. No statistical differences between the two formulations were observed in mechanical performance loss due to aging. These observations comparing the new formulation to the previous one do not raise concerns regarding the performance of the decaBDE-free XLPE in safety-related cable applications.

6. REFERENCES

[1] Polanský, R. and M. Polanská. 2015. "Testing of the Fire-Proof Functionality of Cable Insulation Under Fire Conditions via Insulation Resistance Measurements." *Engineering Failure Analysis* 57: 334–349. https://doi.org/10.1016/j.engfailanal.2015.08.001.

[2] Mead, J. J., Z. Tao, and H.S. Liu. 2002. "Insulation Materials for Wire and Cable Applications." *Rubber Chemistry and Technology* 75: 701. https://doi.org/10.5254/1.3544996 .

[3] EPRI. 2017. *Cable Polymer Material Handbook—Low Voltage Power and Control Cable*. Electric Power Research Institute 3002010637. Palo Alto, CA. https://www.epri.com/research/products/3002010637.

[4] D. O'Hagan. 2008. "Understanding Organofluorine Chemistry. An Introduction to The C–F Bond.", *Chemical Society Reviews* 37(2): 308–319. https://doi.org/10.1039/B711844A.

[5] Henry, J. J., D. Seiler, and R. Perrinaud. 2008. "The "Goods" on Fluoropolymers in Wire and Cable." In *Proceedings 57th International Wire and Cable Symposium (IWCS)*, Providence, Rhode Island, November 9-12, 2008. https://hpp.arkema.com/files/live/sites/shared_arkema/files/downloads/HPP/article-reprints/Extreme-materials/kynar-article-reprints/ar-the-goods-on-fluoropolymers-in-wire-and-cable.pdf.

[6] Morgan, A. B. and J.W. Gilman. 2013. "An Overview of Flame Retardancy of Polymeric Materials: Application, Technology, and Future Directions." *Fire and Materials* 37: 259–279. https://doi.org/10.1002/fam.2128.

[7] Liu, B.-W., H.-B. Zhao, Y.-Z. Wang. 2022. "Advanced Flame-Retardant Methods for Polymeric Materials." *Advanced Materials* 34: 2107905. https://doi.org/10.1002/adma.202107905.

[8] Laoutid, F., L. Bonnaud, M. Alexandre, J.-M. Lopez-Cuesta, and Ph. Dubois. 2009. "New Prospects in Flame Retardant Polymer Materials: From Fundamentals to Nanocomposites." *Materials Science and Engineering: R: Reports* 63: 100–125. https://doi.org/10.1016/j.mser.2008.09.002.

[9] Blum, A. and B.N. Ames. 1977. "Flame-Retardant Additives as Possible Cancer Hazards." *Science* 195: 17–23. https://doi.org/10.1126/science.831254.

[10] Cordner, A., M. Mulcahy, and P. Brown. 2013. "Chemical Regulation on Fire: Rapid Policy Advances on Flame Retardants." *Environmental Science Technology* 47: 7067–7076. https://doi.org/10.1021/es3036237.

[11] S.D. Landry. 2012. "Flame Retardants - Regulatory Issues and Sustainability." In *Fire and Polymers VI: New Advances in Flame Retardant Chemistry and Science*, American Chemical Society, 523–538. https://doi.org/10.1021/bk-2012-1118.ch032.

[12] Brown, P. and A. Cordner. 2011. "Lessons Learned from Flame Retardant Use and Regulation Could Enhance Future Control of Potentially Hazardous Chemicals." *Health Affairs* 30: 906–914. https://doi.org/10.1377/hlthaff.2010.1228.

[13] Environmental Protection Agency (EPA). 2021. Decabromodiphenyl Ether (DecaBDE); Regulation of Persistent, Bioaccumulative, and Toxic Chemicals Under TSCA Section 6(h); Final Rule, Federal Register 86. https://www.federalregister.gov/documents/2021/01/06/2020-28686/decabromodiphenyl-ether-decabde-regulation-of-persistent-bioaccumulative-and-toxic-chemicals-under.

[14] Lassen, C., A. A. Jensen, M. Crookes, F. Christensen, C. N. Jeppesen, A. J. Clausen, and S. H. Mikkelsen. 2014. *Survey of Brominated Flame Retardants*. Danish Ministry of the Environment, Environmental Protection Agency, Denmark. https://www2.mst.dk/udgiv/publications/2014/01/978-87-93026-90-2.pdf.

[15] Weil, E. D. and S.V. Levchik. 2008. "Flame Retardants in Commercial Use or Development for Textiles." *Journal of Fire Sciences* 26: 243–281. https://doi.org/10.1177/0734904108089485.

[16] Environmental Protection Agency (EPA). 2019. *Regulation of Persistent, Bioaccumulative, and Toxic Chemicals Under TSCA Section 6(h)*; Proposed Rule, Federal Register 84. https://www.govinfo.gov/content/pkg/FR-2019-07-29/pdf/2019-14022.pdf.

[17] L.E. Starfield. 2023. *Enforcement Statement Regarding the Prohibition of Processing and Distribution in Commerce of Decabromodiphenyl Ether (DecaBDE)-Containing Wire and Cable Insulation in Nuclear Power Generation Facilities under 40 C.F.R.* § 751.405(a)(2)(ii) Enforcement Statement Regarding DecaBDE 5 2. https://www.epa.gov/system/files/documents/2023-05/Enforcement%20Statement%20Regarding%20DecaBDE%205%202%202023.pdf.

[18] Carra, R. and M. Duvall. 2025. *TSCA Enforcement Discretion for the Nuclear Industry – 8 Lessons for Everyone, Beveridge & Diamond PC (n.d.).* https://www.bdlaw.com/publications/tsca-enforcement-discretion-for-the-nuclear-industry-8-lessons-for-everyone/.

[19] O. US EPA. 2023. *EPA Plans to Extend Compliance Date for Regulation of DecaBDE to Ensure Continuity of Nuclear Power Supply Chain*. https://www.epa.gov/chemicals-under-tsca/epa-plans-extend-compliance-date-regulation-decabde-ensure-continuity-nuclear.

[20] Environmental Protection Agency (EPA), Decabromodiphenyl Ether and Phenol, Isopropylated Phosphate (3:1); Revision to the Regulation of Persistent, Bioaccumulative, and Toxic Chemicals Under the Toxic Substances Control Act (TSCA); Final Rule, Federal Register 89 (2024). https://www.govinfo.gov/content/pkg/FR-2024-11-19/pdf/2024-25758.pdf.

[21] Samaan, N., S. Datta, A. Somani, T.R. McJunkin, B. Li, and A. Medam. 2024. *Value of Nuclear Energy to the Reliability of the North American Power System: Results for Western and Eastern Interconnections*, Idaho National Laboratory INL/RPT-24-79840, Idaho Falls, ID. https://lwrs.inl.gov/content/uploads/11/2024/10/ValueNuclearEnergyReliability.pdf.

[22] D.M. Uhlmann, *Extension to Enforcement Statement Regarding the Prohibition of Processing and Distribution in Commerce of Decabromodiphenyl Ether (DecaBDE)-Containing Wire and Cable Insulation in Nuclear Power Generation Facilities* under 40 C.F.R. § 751.405(a)(2)(ii), (2024). https://www.epa.gov/system/files/documents/2024-09/tsca-decabde-rule-enf-stmt-extension_9-27-24_signed_0.pdf.

[23] EPA. 2020. *Exposure and Use Assessment of Five Persistent, Bioaccumulative, and Toxic Chemicals*, Environmental Protection Agency (EPA); Office of Chemical Safety and Pollution Prevention. https://downloads.regulations.gov/EPA-HQ-OPPT-2021-0202-0004/content.pdf.

[24] J.T. Beeler. 2019. "An Examination of Methods to Determine the Flammability Characteristics of Electrical Cables Exposed to Extended Periods of Radiation in Nuclear Facilities." Doctoral Disseration, University of Tennessee, 2019. https://trace.tennessee.edu/utk_graddiss/5658/.

[25] NRC. 2014. *Expanded Materials Degradation Assessment (EMDA): Aging of Cables and Cable Systems* U.S. Nuclear Regulatory Commission NUREG/CR-7153, Volume 5. Washington, D.C. https://www.nrc.gov/docs/ML1427/ML14279A461.pdf.

[26] Liu, S., S.W. Veysey, L.S. Fifield, and N. Bowler. 2018. "Quantitative Analysis of Changes in Antioxidant in Crosslinked Polyethylene (XLPE) Cable Insulation Material Exposed to Heat And Gamma Radiation." *Polymer Degradation and Stability* 156: 252-258. https://doi.org/10.1016/j.polymdegradstab.2018.09.011.

[27] Liu., S. 2017. "Composition Identification, Aging Mechanisms and Nondestructive Aging Indicator of Commercial Filled Cross-Linked Polyethylene (XLPE) Cable Insulation Materials." Doctoral Dissertation, Iowa State University. https://dr.lib.iastate.edu/handle/20.500.12876/30348.

[28] Fifield, L. S., M.P. Spencer, Y. Ni, D. Li, M.R. Pallaka, T.T. Bisel, A. Zwoster, and M.K. Murphy. 2020. *Sequential Versus Simultaneous Aging of XLPE and EPDM Nuclear Cable Insulation Subjected to Elevated Temperature and Gamma Radiation (Final Results).* Pacific Northwest National Laboratory PNNL-30041 Rev.1. Richland, WA. https://lwrs.inl.gov/content/uploads/11/2024/03/Seq_vs_Sim_Aging_XLPE_EPDM_Nuclear_Cable.pdf.